Structural stability of andesite volcanoes and lava domes

Barry Voight

Email alerting service	Receive free email alerts when new articles cite this article - sign up in the box at the top right-hand corner of the article or click **here**

To subscribe to *Phil. Trans. R. Soc. Lond. A* go to:
http://rsta.royalsocietypublishing.org/subscriptions

Structural stability of andesite volcanoes and lava domes

By Barry Voight

Department of Geosciences, Pennsylvania State University,
University Park, PA 16802, USA (voight@ems.psu.edu)

In tribute to Peter Francis and our colleagues at the Montserrat Volcano Observatory.

> *God send me to see suche a company*
> *Together agayne when need is.*

> (Lord Howard of Effingham)

Slope failures resulting from structural instability of andesitic volcanic edifices can generate mobile debris avalanches that travel long distances down or beyond the flanks of volcanoes. More than 20 major slope failures have occurred worldwide over the past 500 years, a rate exceeding that of caldera collapse. Hazards derive from the debris avalanches themselves, from associated explosive activity that ranges from vertical eruptions (often accompanied by pyroclastic currents) to devastating directed blasts, from associated lahars, and from tsunamis. Collapses of growing lava domes are more frequent, are similar, in many ways, to edifice collapse, and can directly generate devastating pyroclastic currents.

This paper examines some aspects of current understanding of edifice and lava-dome instability. The primary focus of the presentation is on mechanisms and factors associated with collapse, the geometric factors, augmented loading by magma, localized strength reduction by physical and chemical changes (the latter commonly associated with hydrothermal processes), strain weakening, pore-fluid (water or gas) pressure enhancement, retrogressive failure, time-dependent failure, and seismic shaking. Some aspects of material property evaluation, analysis procedures, and implications on monitoring are also discussed. Case examples discussed include edifice instability at Mt St Helens, USA, and Soufrière Hills volcano, Montserrat, the stability of lava spines at Mont Pelée, Martinique, and Lamington, Papua New Guinea, and lava-dome stability at Soufrière Hills. The topics bear on understanding hazardous edifice and dome failures, and the measures to anticipate such failures.

Keywords: edifice failure; volcano collapse; lava domes; stability analysis; numerical modelling; limited equilibrium analyses

1. Introduction

Avalanches generated by collapse of 'andesite' volcanoes, typically ranging from *ca.* 0.5 to 10 km^3 in volume, have travelled as far as 100 km, and have affected areas as large as 1500 km^2 (Siebert 1984, 1996; Siebert *et al.* 1987; Ui & Fujiwara 1993).

About 20 major (by volume) volcano collapses have occurred in the past 500 years. The list expands if one includes events with moderate-sized volumes ranging from tens to hundreds of millions of cubic metres, which, if (relatively) modest in size, are not necessarily modest in their consequences. The 26 December 1997 (Boxing Day) collapse of the Soufrière Hills volcano flank in Montserrat is one such example, and this case is revolutionary in the sense that the failure was anticipated over a year in advance, and materials sampling, testing and analyses were carried out before the failure occurred.

Edifice collapse on active volcanoes can be accompanied by magmatic activity and can trigger explosive volcanism, as at Mt St Helens, USA, in 1980, Bezymianny in 1956, and Shiveluch in 1964, both in Kamchatka, Russia, and Soufrière Hills, Montserrat, in 1997, among others (Voight *et al.* 1981, 1983; Gorshkov 1959; Belousov 1995; Belousov *et al.* 1999; Sparks *et al.* 2000). In other cases, phreatic explosive activity has accompanied slope failure, as at Bandai, Japan, and Ritter Island, Papua New Guinea, both in 1888 (Sekiya & Kikuchi 1889; Yamamoto *et al.* 1999; Johnson 1987); and in still other cases, partial edifice failures have been unaccompanied by coeval volcanism, as at Ontake, Japan (Oyagi 1987; Voight & Sousa 1994). Various styles of failure are possible; most involve primarily the volcanic edifice, but in some cases sub-volcanic basement spreading may be involved, as at Mombacho volcano, Nicaragua, and Socompa, Chile (Van Bemmelen 1949, 1950; Francis 1993; Francis *et al.* 1985; Francis & Self 1987; Wadge *et al.* 1995; Van Wyk de Vries & Borgia 1996; Van Wyk de Vries & Francis 1997; Van Wyk de Vries *et al.* 1999). Some comparative cross-sections are shown in figure 1. Certain characteristics of failed volcanoes are reviewed by Siebert (1996); causes of collapse are reviewed by Voight & Elsworth (1997, table 1). The percentage of volcanoes that have collapsed correlates with volcano height: increasing from less than 10% of volcanoes under 500 m high to more than 75% of volcanoes over 2500 m high in the central Andes (Francis & Wells 1988; Naranjo & Francis 1987; De Silva & Francis 1991). Avalanche run-out is conditioned by failure volume (Voight *et al.* 1985; Siebert 1996; Dade & Huppert 1998). Associated hazards may include catastrophic waves from interaction with oceans or lakes (Slingerland & Voight 1979; Kienle *et al.* 1987; Siebert *et al.* 1987; Tinti *et al.* 1999). Obviously, collapsing volcanoes and associated explosions or water waves are extremely hazardous, and, during the past 400 years, more than 20 000 people have been killed by avalanches or closely related events (lahars excluded).

All of the volcanoes referred to above are, in a very general sense, 'andesite' volcanoes, with lava compositions in the neighbourhood of 60% SiO_2 (i.e. mainly basaltic andesites to dacites). All are polygenetic, having experienced more than one eruptive episode in their history. Most are composed of a relatively steep, roughly conical stack of lavas and interbedded pyroclastics and palaeosols. In this sense, formed of distinct parts or substances, they are *composite* (Williams & McBirney 1979), and also in the sense of implying evolution complexity (Francis 1993, p. 350). Some andesite volcanoes are formed primarily of overlapping lava domes and short thick flows (*coulées*), and associated breccias, forming composite domes or dome complexes (e.g. Shiveluch and Augustine; see Belousov *et al.* (1999), Beget & Kienle (1992) and Siebert *et al.* (1995)), whereas others are dominantly formed of longer lava-flow tongues and interbedded clastic material, and some, like Mt St Helens, are partly formed of interbedded lava and tephra units punctured by localized flank and summit domes. The edifices may also contain, from time to time, injections of fresh magma. The
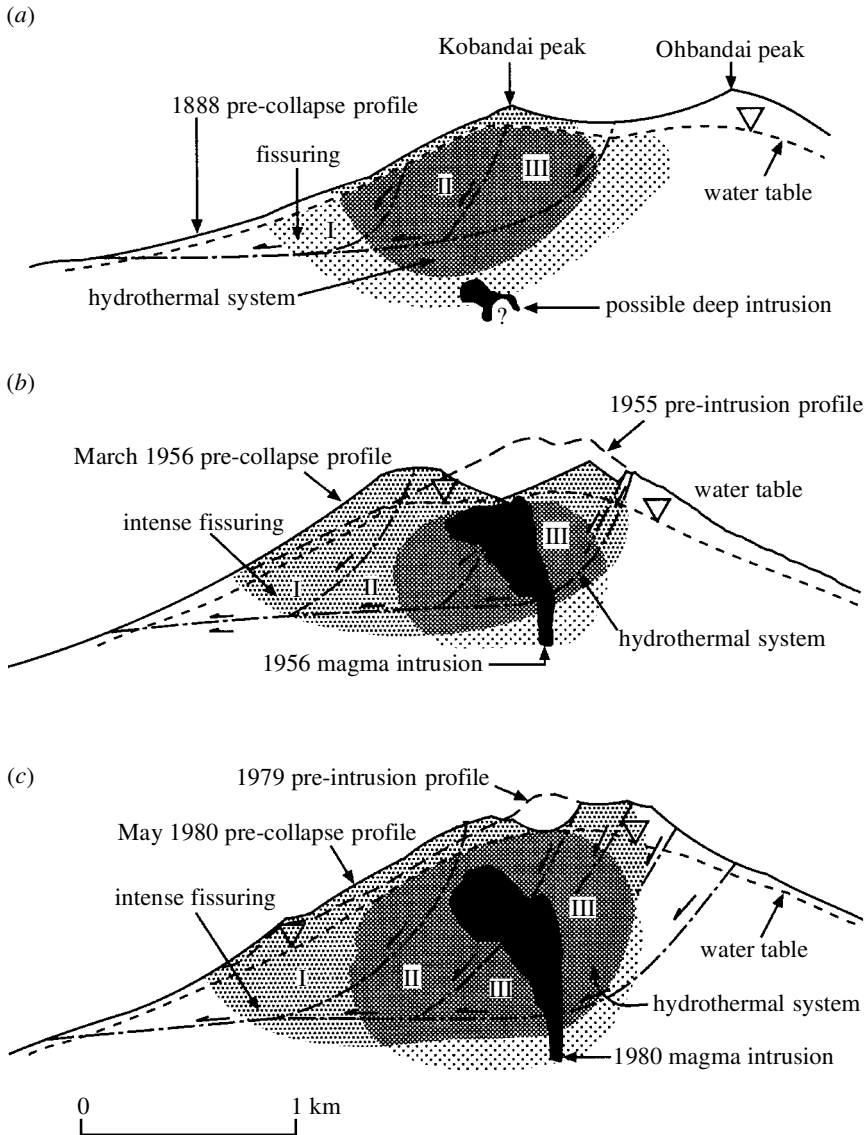
Figure 1. Schematic cross-sections of composite volcanoes associated with major edifice collapse: (*a*) Bandai, 1888; (*b*) Bezymianny, 1956; (*c*) Mt St Helens, 1980 (after Voight & Elsworth 1997). In all three cases collapse is interpreted as retrogressive failure of successive blocks, indicated by roman numerals. Magma intrusions promoted the collapse of (*b*) and (*c*). The depths of the avalanche scars are attributed to fragmental, highly fissured, or altered material in the volcano cores, and to the fluidized nature of these materials in association with overpressurized hydrothermal and magmatic systems. Fault structures associated with magma emplacement are not shown.

common hallmark of such cones is that the material properties vary substantially from place to place. Thus, the andesite volcano edifice is typically heterogeneous and anisotropic, and its material properties are quite complex.

This paper considers the various causes of edifice collapse, and develops a generalized mechanical analysis to underscore the qualitative significance of important factors leading to collapse. The role of magma is explored in relation to its direct influence on the driving forces, tending to destabilize the edifice, and also to its indirect influence on pore-fluid pressures. Pore-fluid (liquid and gas) pressures affect the frictional resistance of edifice materials, and, in some cases, also affect the driving forces. Some aspects of material property evaluation, analysis procedures, and implications on monitoring are then discussed. Case examples discussed include edifice instability at Mt St Helens, USA, and Soufrière Hills volcano, Montserrat; the stability of lava spines at Mont Pelée, Martinique, and Lamington, Papua New Guinea; and lava-dome stability at Soufrière Hills. The topics bear on understanding hazardous edifice and dome failures, and the measures to anticipate such failures. For those scientists obliged to provide guidance for decisions in such matters, the responsibility can be daunting. The aim of this paper is to make their path somewhat easier.

2. Mechanical models for edifice and dome failures

(a) Fundamental aspects of instability

Evaluations of edifice or flank instability are carried out for the purpose of hazards appraisal at a given site, or to understand a failure that has already occurred. Although the expectations can be different, both questions can be approached by

(i) examining the past history of the site, which may have involved prior failures that provide insight to current developments (see, for example, Beget & Kienle 1992; Belousov *et al.* 1999);

(ii) comparing events developing at one volcano with well-studied potential analogues elsewhere (e.g. the comparison of Mt St Helens in April 1980 with Bandai San, Japan, in 1888; see Voight (1980));

(iii) carrying out a geomechanical analysis, involving site characterization of geometry and materials distribution, characterization of material properties and conditions (including fluid pressure distributions, seismic loading), and analytical or numerical modelling (Voight *et al.* 1983; Paul *et al.* 1987; Iverson 1995; Voight & Elsworth 1997); or

(iv) observational monitoring of the edifice (e.g. displacement, tilt, seismic strong motions, propagation and widening of visual cracks, etc.) (Voight & Kennedy 1979; Pariseau & Voight 1979; Lipman *et al.* 1981; Moore & Albee 1981; Voight *et al.* 1983, 1987, 1989; Voight 1979, 1988, 1989, 1992; Murray *et al.* 1994; McGuire *et al.* 1995; Scarpa & Tilling 1996).

Slope instability can be discussed conveniently by considering the forces parallel to the surface (or zone) of sliding. The sliding mode of failure is emphasized here, but other modes such as toppling are possible. The total force driving outward movement, S, is opposed by the resisting shear force, T, mobilized along a potential basal slide surface and lateral boundaries. T represents the integrated value of mobilized shear resistance, s, over the area of failure. The shear resistance is commonly defined in terms of effective-stress Coulomb strength parameters, cohesion, c', and friction

angle, ϕ', whereby $s = c' + \sigma' \tan \phi'$, and the primes signify parameter correspondence to *effective stresses* σ' (i.e. total stress minus pore-fluid pressure). In simple terms, imagined most readily as a wedge sliding on a plane surface, the mobilized shear force T is equal to $(c'A + N' \tan \phi')$, where N' is the 'effective' normal force perpendicular to the failure surface of area A. A factor of safety, F_s, can be defined as $F_s = T/S$. (Another way of expressing the concept is that F_s is the factor by which the shear strength must be divided to bring the slope to the verge of failure (Duncan 1996; Bishop 1955).) At failure, the components of the outward disturbing force, S, and mobilized shear force, T, are, by definition, equivalent.

The force components normal and parallel to the failure surface can be more or less readily assembled to produce an equation of stability in terms of the fundamental factors, such as configuration of the potential failure surface (the most critical surface must generally be selected, or 'located', by trial and error), weight of the failing block, uplift forces of pressurized pore fluids, 'downward' force by seawater for oceanic volcanoes, forces associated with magmatic injection (or other fluids), seismic loads, and forces representing the strength of the materials (Voight & Elsworth 1997). Of these terms, some are easily obtained (e.g. block weight), whereas others may be difficult or impossible to measure reliably (e.g. rock-mass strength, dynamic loading, the constitutive properties of partly crystalline magma), but, in general, some limiting bounds can be placed, and the influence of the primary variables can be examined through sensitivity analyses.

This form of analysis is adequate to guide some understanding of the relative significance of the controlling parameters, and this is useful. On the other hand, analysis is not adequate to enable the *reliable* and accurate computation of the factor of safety of a given edifice or slope, because complete information on distributions of materials (complex geology), rock-mass and magma strength and deformation properties, edifice stresses, discontinuities cannot be reliably obtained. Emphasis above is on the word *reliable*. In some cases, *reasonable estimates* may be placed on properties, but some relatively small variations of, let us say, cohesion c'—well within the limits of uncertainty—can have quite an important influence on the computation. This is a strong limitation imposed by a realistic view of the field situation, rather than one imposed by the methods of analysis, which are becoming quite sophisticated. For this reason, when concern is expressed concerning edifice stability, there is no substitute for observational monitoring. The early signs of instability may include cracking near the crest of the slope, and outward bulging near the toe, and *such signs, and the monitored evolution of the deformation field, are of more importance than any theoretical analysis that is, necessarily, based on assumed or laboratory-measured values.* This is not to argue that materials testing is not helpful. It is all a matter of perspective and good judgment.

For a slope that has remained stable throughout a volcanic–seismic crisis, it is usually impossible to calculate a reliable value of F_s other than to note that it exceeds unity. As Duff Cooper might put it:

> . . . it is impossible now, to form an accurate estimate of the danger. The misfortunes we escape cannot be measured, nor can the margins by which we escape them.

Also, stability analyses may be performed to constrain by 'back analysis', assuming $F_s = 1$, the field shear strengths at failure from the study of selected case histories, for
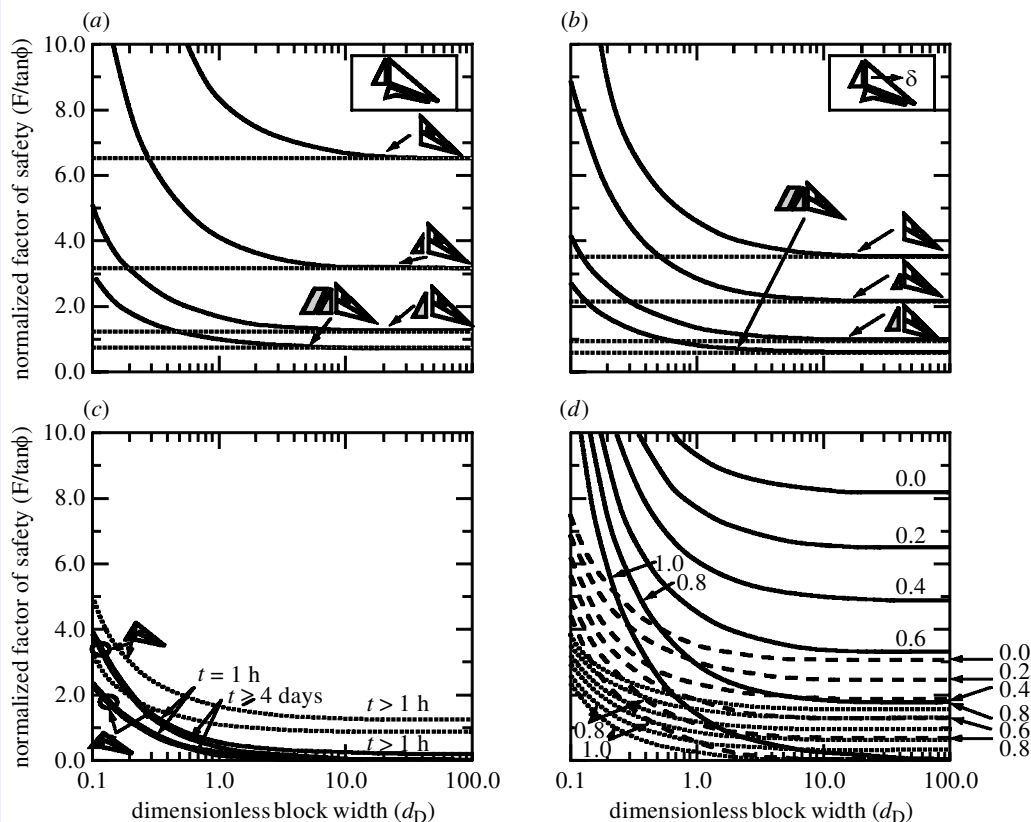
Figure 2. Normalized factor of safety for failure of a composite volcano flank with (a) static groundwater force, $K_0 = 0$ (dotted curve) and 0.5 (solid curve) for zero magma loading, half-depth dyke penetration, full-depth dyke penetration, and full-depth dyke penetration with overpressure. (b) Same as (a) but for seismic loading coefficient $= 0.1g$. (c) Same as (a) but for thermally induced pore pressure resulting from fully penetrating dyke, with static piezometric conditions as noted. (d) Same, for fluid uplift pressures β of 0.0–1.0. Solid lines: zero magma loads, static case. Dashed lines, zero magma loads, seismic coefficient $= 0.2g$. Dotted lines: magmastatic loads, static case (after Voight & Elsworth 1997).

which the failure geometry and some other parameters may be 'relatively' well under-stood. However, the existing 'avalanche caldera' should not generally be assumed to represent the critical shear surface used for stability analysis, because volcano edifice failure is commonly retrogressive (Voight *et al.* 1983; Voight & Elsworth 1997), and the resulting caldera form is often influenced by multiple failures and evacuation of fluidized material, or by localized explosions, that followed the initial, generally rotational, failure along a critical shear surface of steeper average inclination than the final caldera. This is an attribute of flowslides generally, whereby the initial fail-ure mass possesses sufficient mobility to remove itself from the site of failure, thus clearing the path for further slices of material to fail in succession.

In the following series of analyses, models with applied magmatic forces simulate Bezymianny-type collapse with upper-edifice intrusions; analyses lacking such forces simulate Bandai-type collapses or those that trigger eruption from deeper magma

sources (e.g. Shiveluch in 1964), or mass movement types unaccompanied by eruptions (e.g. Ontake). The geometry chosen is a flank rising at $30°$, a static groundwater surface rising from the toe at $18.5°$, and a wedge-shaped block with a basal failure surface dipping outwards at $7°$. (The flat basal surface is selected only for mathematical convenience, because curved or partly curved surfaces are likely in nature due to kinematic requirements, except where a very weak planar stratum controls the geometry of failure.) Results are presented as factors of safety normalized by $\tan \phi'$, against dimensionless block width, d_D, where d_D is the ratio of the failure block width to slope height above sea level (Voight & Elsworth 1997). Thus, the results are for a three-dimensional block, with d_D a measure of width of the failure plane. The influence of side-wall strength can be important for narrow block widths, but, as width increases, the two-dimensional solution is approached. K_0 is lateral earth pressure that controls the normal stress on side boundaries; for $K_0 = 0$, lateral restraint is discounted. (Note that the reader may substitute arbitrary values for ϕ'; e.g. for $\phi' = 27°$, $\tan \phi' = 0.5$, and, thus, if $F_s / \tan \phi' = 2$, then $F_s = 1$, implying failure.)

Four cases of rear-scarp loading are used for a sensitivity evaluation:

  (i)   zero magma loading;

 (ii)   half-depth magma penetration;

(iii)   full-depth magma penetration; and

(iv)   full-depth penetration with overpressure.

Both the normalized factor of safety and the influence of lateral restraint decrease as magma pressures increase (figure $2a$). Failure is feasible at nominal values of ϕ' for a fully penetrating intrusion. For modest values of K_0, the block width should equal or exceed depth to the failure surface ($d_D > 1$). This result is consistent with the data of Siebert *et al.* (1987): out of 106 datasets, only four reported widths were less than 1 km.

For the same four cases, stability is evaluated for a uniform lateral seismic acceleration of $0.1g$. The influence is to reduce stability (figure $2b$), with the changes most significant for partial penetration and zero edge loading. For the former (in weak materials), failure is feasible for $d_D > 3$; for the latter, supplementary loads are needed for failure. The results are qualitatively consistent with historical failures at Miyuyama, Bandai, Bezymianny, Shiveluch and Mt St Helens, all of which were associated with earthquakes with magnitudes around five (Okada 1983; Siebert *et al.* 1987).

Likewise, fluid pressures generated thermally by an intrusion affect stability (figure $2c$; see also Elsworth & Voight (1995); Voight & Elsworth (1997)). Other conditions are represented by figure $2d$, in which generalized piezometric conditions are indicated by the ratio, β, of total fluid uplift force on the slide plane to the normal component of overburden weight. These generic curves apply to any piezometric condition, irrespective of causative mechanism (e.g. pore-fluid enhancement by thermal intrusion, retrograde boiling (magma degassing), hydrothermal systems, seismicity-induced strain).

The results confirm that Bezymianny-type failures with magmatic loads are feasible with conventional groundwater piezometry and nominal ϕ' values. For the static
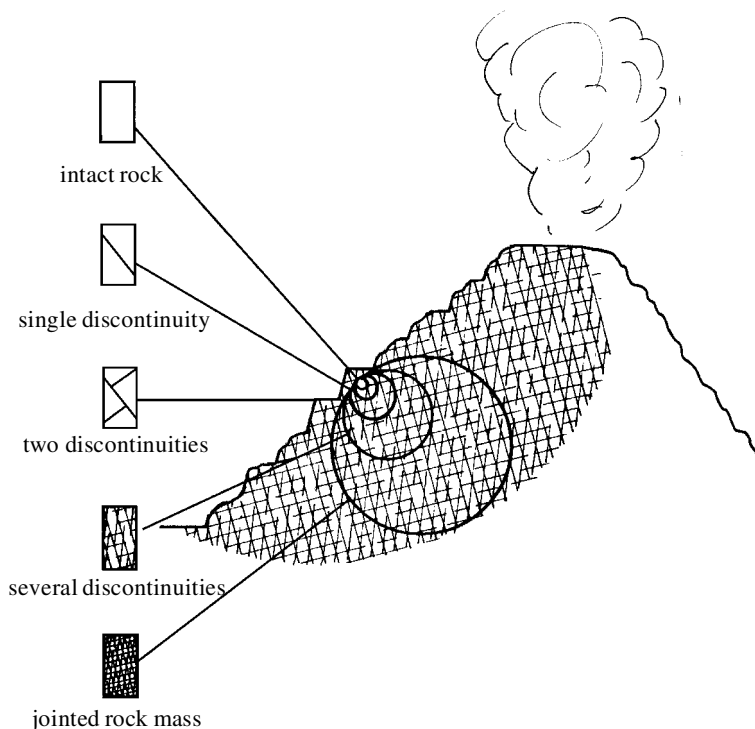
Figure 3. Simplified representation of the influence of scale on the type of rock-mass behaviour model that should be used in simulating volcano slope behaviour (after Hoek 1983).

case, high fluid uplift values are needed ($\beta > 0.8$). Where fluid pressures are already moderately elevated, earthquake loading can clearly trigger failure.

On the other hand, hydrothermal systems and volcanic crises involving repetitive magmatic intrusions and eruptions are more common on volcanoes than are massive slope failures; this comparison suggests that stringent requirements involving combinations of mechanisms and materials are necessary to produce major failures.

(b) Strength properties for volcanic masses

One of the major problems in volcano stability analyses is in estimating the strength and deformation properties of the volcanic mass, which consists of relatively intact material separated by structural discontinuities. A similar problem is faced by engineers in designing an underground or surface excavation. It is practically impossible to carry out triaxial or shear tests on rock masses *at a scale that is appropriate* for these problems.

The engineering approach has been to develop and use an empirical failure criterion with intact or heavily fractured, relatively isotropic rock masses (figure 3; see also Hoek & Brown (1980, 1988), Hoek (1983) and Hoek *et al.* (1992)). In its most general form, the Hoek–Brown criterion is given by

$$\sigma_1' = \sigma_3' + \sigma_c\{m_b(\sigma_3'/\sigma_c) + s\}^a,$$

where m_b, s and a are constants that depend upon the composition and characteristics of the rock mass, σ_c is the uniaxial compressive strength of the intact rock,

and σ_1' and σ_3' are the axial and confining effective principal stresses, respectively. The material constants are estimated by rock-mass classifications, such as the 1976 version of the Bieniawski (1989) rock mass rating, or the geological strength index (GSI) of Hoek *et al.* (1994). Thus, $m_b = m_i \exp\{GSI - 100)/28\}$, where m_i is the m-constant for intact rock, about 19 for *andesite*, and $s = \exp\{(GSI - 100)/9\}$, for GSI > 25 (table 1). Similar correlations have been devised to estimate near-surface deformation modulus E_m.

These criteria are purely empirical, and there is no fundamental relation between the empirical constants and any physical characteristics of the rock. The justification for choosing the Hoek–Brown criterion over some others lies in the apparent adequacy of its predictions of observed rock-fracture behaviour and the convenience of application. As indicated earlier, many numerical models or limit equilibrium analyses are expressed in Coulomb parameters, and these can be established for a given set of Hoek–Brown parameters by the expressions

$$\sigma_n' = \sigma_3' + \frac{\sigma_1' - \sigma_3'}{(\delta\sigma_1'/\delta\sigma_3') + 1}$$

and

$$\tau = (\sigma_n' - \sigma_3')\left(\frac{\delta\sigma_1'}{\delta\sigma_3'}\right)^{0.5}.$$

The Hoek–Brown criterion results in a curved strength envelope as a function of confining pressure, in contrast to the linear Coulomb relation. Geological media tend to have nonlinear strength envelopes, and the linear Coulomb relation, if fitted to data at higher normal stress levels, commonly overestimates the available shear strength at low confining pressures and can result in unrealistic ratios of tensile strength to uniaxial compression strength. The converse situation applies for fits to data at lower confining pressures. The resulting errors on factors of safety or the theoretical development of zones of plasticity can be appreciable (Pariseau *et al.* 1970; Hoek 1983).
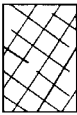
One may infer that a curvilinear or piecewise-linear yield function is a necessity for a stability analysis, or an elastic–plastic analysis, where results cannot be fully anticipated by intuition. This illustrates the importance of considering test data in relation to the effective normal stress levels that occur in the problem being evaluated, and recognizing the dilemma that can occur with use of Coulomb parameters when the occurrence of both high and low normal stresses are important to the solution. Another aspect of the question involves the independent measurement of solid friction and dilatancy coefficients for such materials, a topic that appears in relation to non-associated flow rules, important in numerical modelling (Vermeer & De Borst 1984).

(c) Magma properties

Magma properties vary from those of a hydrated crystal-rich material at depth, with a Newtonian viscosity commonly of the order 10^6 Pa s, to those of degassed crystalline lava in the edifice, with a more complex rheology that can be approximated by an apparent viscosity of more than 10^{13} Pa s and a (Bingham) yield strength of more than 1 MPa (Voight *et al.* 1999). Physical properties of silicic magmas have been reviewed by Alidibirov *et al.* (1997) and Dingwell (1998). The melt phase of

Table 1. *Estimation of strength and deformation constants for rock mass*

(Estimation of m-constants for rock mass (m_b) and intact rock (m_i), constants a, s, deformation modulus E_m and Poisson's ratio ν for the generalized Hoek–Brown failure criterion based upon rock mass structure and discontinuity surface conditions (after Hoek *et al.* 1994). Values given are for an undisturbed rock mass. Units of E_m are MPa.)

GENERALIZED HOEK–BROWN CRITERION

$$\sigma_1' = \sigma_3' + \sigma_c \left(m_b \frac{\sigma_3'}{\sigma_c} + s \right)^a$$

σ_1' = major principal effective stress at failure

σ_3' = minor principal effective stress at failure

σ_c = uniaxial compressive strength of *intact* pieces of rock

m_b, s and a are constants which depend on the composition, structure and surface conditions of the rock mass

STRUCTURE	SURFACE CONDITION	VERY GOOD very rough, unweathered surfaces	GOOD rough, slightly weathered, iron stained surfaces	FAIR smooth, moderately weathered or altered surfaces	POOR slickensided, highly weathered surfaces with compact coatings or fillings containing angular rock fragments	VERY POOR slickensided, highly weathered surfaces with soft clay coatings or fillings
BLOCKY — very well interlocked undisturbed rock mass consisting of cubical blocks formed by three orthogonal discontinuity sets	m_b/m_i	0.60	0.40	0.26	0.16	0.08
	s	0.190	0.062	0.015	0.003	0.000 4
	a	0.5	0.5	0.5	0.5	0.5
	E_m	75 000	40 000	20 000	9000	3000
	ν	0.2	0.2	0.25	0.25	0.25
	GSI	85	75	62	48	34
VERY BLOCKY — interlocked, partially disturbed rock mass with multifaceted angular blocks formed by four or more discontinuity sets	m_b/m_i	0.40	0.29	0.16	0.11	0.07
	s	0.062	0.021	0.003	0.001	0
	a	0.5	0.5	0.5	0.5	0.53
	E_m	40 000	24 000	9000	5000	2500
	ν	0.2	0.25	0.25	0.25	0.3
	GSI	75	65	48	38	25
BLOCKY/SEAMY — folded and faulted with many intersecting discontinuities forming angular blocks	m_b/m_i	0.24	0.17	0.12	0.08	0.06
	s	0.012	0.004	0.001	0	0
	a	0.5	0.5	0.5	0.5	0.55
	E_m	18 000	10 000	6000	3000	2000
	ν	0.25	0.25	0.25	0.3	0.3
	GSI	60	50	40	30	20
CRUSHED — poorly interlocked, heavily broken rock mass with a mixture of angular and rounded blocks	m_b/m_i	0.17	0.12	0.08	0.06	0.04
	s	0.004	0.001	0	0	0
	a	0.5	0.5	0.5	0.55	0.60
	E_m	10 000	6000	3000	2000	1000
	ν	0.25	0.25	0.3	0.3	0.3
	GSI	50	40	30	20	10

crystal-rich andesitic magmas is rhyolite, and viscosity estimates can use the relations of Hess & Dingwell (1996). Strength parameters for high-temperature, partly molten magmas are poorly known. Failure angles of around 40° from maximum compression direction are reported for high-temperature compression tests on andesite,

which suggests friction angles of the order of 10°. Creep tests at 900 °C have been conducted on degassed crystalline andesite lava by A. M. Lejeune, but results have not yet been published.

3. Analysis methods

Two general procedures are used to evaluate slope stability: limit equilibrium analyses and deformation analyses. Major strides have been taken in both areas over the past three decades, largely because of the availability of microcomputers. Both topics are examined here.

(a) *Limit equilibrium analyses of stability*

Computing power now enables use of 'advanced' limit equilibrium analysis (LEA) methods that satisfy most or all conditions of equilibrium, and a large number of trial circular or non-circular slip surfaces can be analysed, making it possible to identify critical slip surfaces with a relatively high degree of reliability. The principles underlying LEA are as follows:

(i) a slip mechanism is postulated;

(ii) the shearing resistance required to equilibrate the slip mechanism is calculated by statics;

(iii) this calculated resistance is compared with available shear strength in terms of factor of safety F_s;

(iv) the procedure is repeated for other postulated mechanisms, and the lowest F_s is found by iteration.

Many LEA methods have been developed, and the analyst needs to know which of these methods are accurate, which can develop convergence problems or other numerical problems, and which of the accurate methods can be applied most easily. Some comparative evaluations have been published (Duncan & Wright 1980; Fredlund 1984; Nash 1987; Duncan 1992, 1996).

The number of available equations of equilibrium is smaller than the number of unknowns in stability problems. Thus, all LEA methods employ assumptions to make the problem determinate. In the case of methods that satisfy all conditions of equilibrium, the assumptions do not have a significant effect on factor of safety. However, for LEA methods that satisfy force equilibrium and not moment equilibrium, F_s is affected significantly by the assumed inclinations of side forces between adjacent slices. Some studies have considered the computational accuracy of various methods, comparing calculated F_s values with 'what are believed to be' the correct answers for a given slope geometry and set of material properties. The theoretical 'correct' answer can be defined to a level of accuracy of at least ±6%, which is considered adequate because material properties selected for a real slope cannot match this accuracy. In such evaluations, the minimum values of F_s for different LEA methods are usually compared, because different methods can result in different critical slip surfaces. If the F_s results are compared for arbitrarily chosen slip surfaces, the results of the comparison depend on which surface is selected; this is disconcerting, since

identification of the critical surface position and geometry may be considered to be important as the critical value of F_s.

As a result of these comparisons, the relative merits and demerits of various LEA methods are relatively well understood. As LEA methods of varied reliability are available in commercial codes, it behoves the user to evaluate which of these methods is sufficiently adequate for the intended purpose. Various LEA codes are available with search routines for locating the critical circular slip surface, which is relatively straightforward, although, in some instances, local F_s minima can occur. The problem of locating the critical non-circular surface is more complex, but some progress has been made. Unless there are geological controls that constrain failure development, the critical slip surface will be nearly circular (Spencer 1981; Duncan 1992). Arcuate, nearly circular failure surfaces were interpreted for the initial slide blocks at Mt St Helens, Bandai and Bezymianny volcanoes (Voight & Elsworth 1997). However, it is not uncommon for geological controls (weak strata, etc.) to be significant in volcano failures, as at Ontake, Japan (Voight & Sousa 1994). When the failure surface is non-circular, internal deformation of the slide mass occurs due to kinematic requirements. The stability method of Sarma (1979) allows non-vertical slices and can be useful for such cases, and for those in which non-vertical structures cross the slide mass.

Two-dimensional LEA is now relatively mature, but the same cannot be said for three-dimensional analysis (Morgenstern 1992). A number of three-dimensional slope stability methods have been developed (Duncan 1992), but some problems have been recognized. For example, some three-dimensional LEA methods have been based on an extension of the 'ordinary method of slices', which is known to be inaccurate for effective stress analyses. The most useful solution to date appears to be that of Hungr (1987; Hungr *et al.* 1989), which is based on an extension to three dimensions of Bishop's simplified method of analysis in which the vertical inter-column shear forces are neglected. A similar procedure has recently been followed by Reid *et al.* (2000), in combination with a digital elevation model (DEM) and a three-dimensional search grid of points above the DEM, to represent the centre of rotation of a set of spherical trial slip surfaces of different radii. The procedure enables determination of minimum stability at each DEM grid point, and also the volume associated with each critical surface. The method was applied to idealized strato-volcanoes and tested for the case of 1980 Mt St Helens.

(b) *Deformation analyses*

This brief review focuses on numerical analyses employing finite-element or finite-difference procedures, which have many desirable attributes for evaluating stresses, movements, cracking and fluid pore pressures in slopes. The literature is extensive, and the procedures have been used for slope stability analyses for about three decades (Brown & King 1966; Morgenstern 1992; Duncan 1992, 1996). Materials are represented by zones or elements, which form a grid that can be adjusted to fit the shape to be modelled. Each element behaves according to a prescribed linear or nonlinear constitutive law in response to applied forces or boundary restraints. In the finite-element method (FEM), the field quantities (stresses, displacements) vary throughout each element in a prescribed fashion, using functions controlled by parameters. The formulation consists of adjusting these parameters to minimize error terms on local or global energy. In contrast, in the finite-difference method (FDM), each derivative in

the set of governing equations is replaced directly by an algebraic expression written in terms of the field variables at discrete points in space. Both methods produce a set of algebraic equations, and it can be shown in specific cases that the resulting equations are identical, despite the different derivation procedures. Thus, it is futile to debate the relative merits of the FEM versus the FDM, as the outcome can be exactly the same. However, because of traditions, certain features are more commonly associated with one method than with another. Thus, implicit, matrix-based solution schemes are more common with the FEM, whereas explicit, time-marching solution methods are practical for the FDM. Likewise, various commercial or freeware codes are available for each of these general methods, and the specific features offered by these codes vary widely in sophistication. Not all are especially suitable for geotechnical applications.

Numerical codes offer the possibility of extending rational continuum approaches to complex (and changing) geometries and material behaviours, in heterogeneous media, with isotropic and anisotropic options, a variety of nonlinear constitutive models, and interface models to simulate fault slip or joint separation (Barton & Bandis 1982, 1990; Cundall & Board 1988; Duncan 1992, 1996; Goodman *et al.* 1968; Sleep 1999; Vermeer 1991; Wang & Voight 1969). The range of application of rational mechanics is extended by two- and three-dimensional discontinuum codes, which allow consideration of the behaviour of assemblages of discrete discontinuities (Cundall 1980, 1990; Pouyet *et al.* 1983; Hart *et al.* 1988; Mustoe 1989). *Path dependency*, whereby the final field quantities depend upon the manner in which the applied loads reach their final values (Pariseau *et al.* 1970), is an important consideration, particularly where sequential addition or removal of material is modelled (Desai & Abel 1972; Duncan 1992). The appropriateness of some plastic and creep constitutive equations remains a lingering issue (Pariseau *et al.* 1970; Voight & Dahl 1970; Zienkiewicz *et al.* 1975), but viable associated and non-associated strain-strengthening and strain-weakening constitutive models have been developed for Mohr–Coulomb, Cam clay-type, and other materials (Pietruszczak & Mroz 1981; Vermeer & De Borst 1984; Drescher & Mroz 1997). Incremental analyses provide a convenient means of modelling changes in geometry and nonlinear behaviour (Desai & Abel 1972; Duncan 1996). Pseudo-static loading to represent seismic loads can be used usefully in numerical codes, as they are in LEA, although the limitations of the method have been recognized since its infancy (Terzaghi 1950; Seed 1979). Some numerical codes enable explicit simulation of dynamic loads (Finn *et al.* 1986; Finn 1988; Succarieh *et al.* 1991; Byrne *et al.* 1992). The analysis of slopes under seismic loading generally follows the procedures used for static slope stability, but is further complicated by the effects of dynamic stresses induced by earthquake shaking, and the effects of those stresses on the strength and stress–strain behaviour of the slope materials.

A factor of safety can be calculated with an FEM or FDM code by reducing material strength in stages until failure occurs. This 'shear-strength-reduction technique' has some advantages over traditional LEA methods (Zienkiewicz *et al.* 1975; Ugai & Leshchinsky 1995). The critical failure zone is found automatically; it is not necessary to specify the shape of the failure surfaces, and failure mechanisms such as deforming wedges can be analysed.

At the current stage of development, simulation is firmly embedded within the observational method, and is an essential tool in assisting the practitioner to evaluate

the information available. Nevertheless, there are limitations. When the factor of safety is high, the results from numerical studies can be accurate *if* (a big *if*!) media properties are known reliably (Morgenstern 1992). At low stress levels, the strains that result from an increment of stress are calculated relatively accurately by elastic stress–strain relations. However, as F_s decreases, the extent of yielding increases, and the ability of many codes to simulate reality decreases. Strain weakening is the main reason for the localization of shear deformation within a yielding rock mass into a discrete slip surface, apart from geological zonation in heterogeneous material, which predefines the shear band (Wiberg *et al.* 1990), but computation of stress-induced localization within a strain-weakening material remains a complex topic. Also, regarding constitutive relations, the Hoek–Brown method has been little used in numerical modelling because of certain difficulties in developing a reliable flow rule to supply a relation between the components of strain rate at yield (Shah 1992; P. Cundall, personal communication).

The philosophy of numerical modelling of volcanic systems must be very different from, say, structural engineering, for it is impossible to obtain complete field data (material zonation, discontinuities, properties, stresses) at a volcanic site. In the typical situation, the volcanic system is extremely complicated and nonlinear, but miniscule funds and opportunities exist for geotechnical site investigation (boreholes, etc.), the testing budget is small to non-existent, and most materials could not be 'tested' reliably even if funds were available. Under these circumstances, as proposed by Starfield & Cundall (1988) for rock-engineering sites, numerical modelling should be used mainly to give insight into *mechanisms*. Under more favourable field and budget conditions, sometimes available in volcanology, modelling may be used to bracket field behaviour through parametric studies (only some values of the assumed parameters will give results that are consistent with observations), and, in more rare circumstances, may be used for prediction.

4. Case examples

(a) Stability of Mt St Helens, May 1980

The eruption of Mt St Helens in 1980 is the best-documented edifice failure (Lipman & Mullineaux 1981). The volcano became active in late March 1980, with substantial shallow seismic activity concentrated on the north flank. Visual observations indicated that a fracture system, defining a graben, crossed the summit area, and that large deformations affected most of the north flank. The relation of the fracture systems and deformation to potentially hazardous rockslides and glacier slides was recognized by early April (figure 4; see also Voight (1980), Decker (1981), Miller *et al.* (1981) and West (1980)). Voight's 1 May report on stability hazards (see report included at the end of this paper) suggested that a rockslide triggered by hydraulic pressures in weak fragmental layers and release of seismic energy 'could be as much as a kilometre thick and involve a cubic kilometre or more of rock and fragmental material', and cited as an analogue the 'explosively motivated fragmental flow' observed at Bandai-San in 1888 (Sekiya & Kikuchi 1889). The report noted the possibility for high emplacement avalanche velocities (67–96 m s^{-1}) and long runout, lake tsunami hazards, lahars and depressurization-caused explosions in hydrothermal systems, and also, perhaps, shallow magma chambers. Ground displacement surveys initiated in late April confirmed that subhorizontal displacements were as much as 1.5–2.5 m d^{-1}
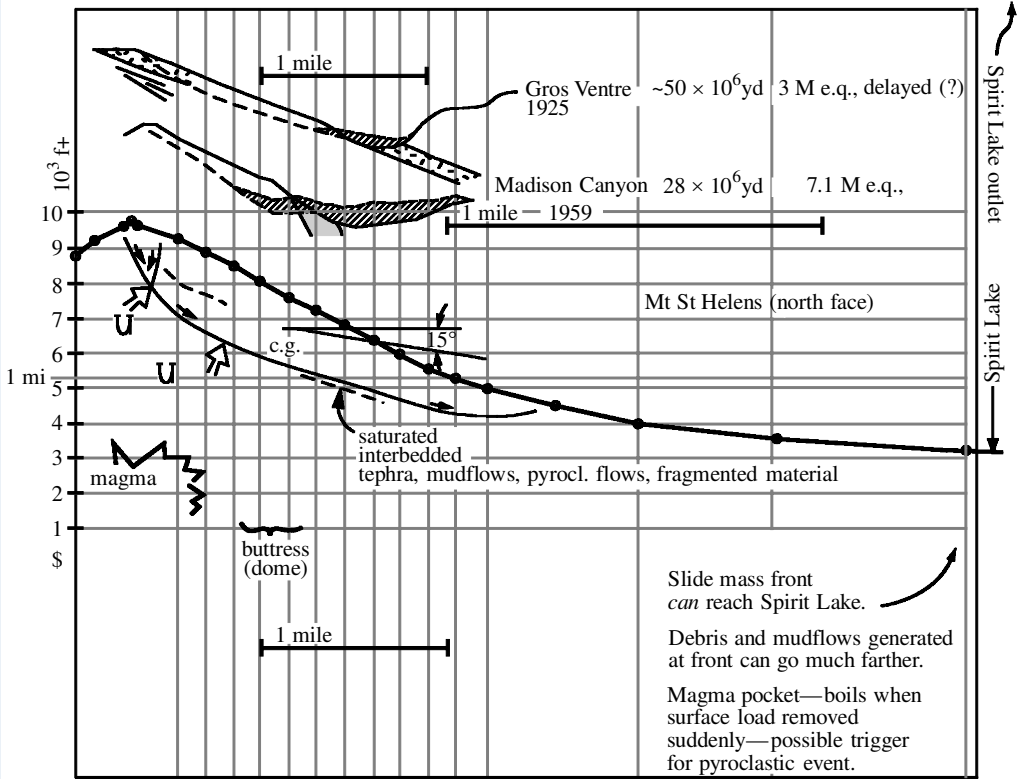
Figure 4. Slope hazards assessment diagram posted 15 April 1980 by B. Voight at USGS headquarters in Vancouver, Washington, comparing Mt St Helens with two well-studied earthquake-triggered landslides. Simple calculations suggested a potential slide volume of as much as $3\ \mathrm{km}^3$.

(Lipman *et al.* 1981). No measurements or estimates of rock strength were made during this period, nor were quantitative stability analyses developed. It was believed that observational monitoring of slope performance was more relevant than any stability assessment using parameters of highly uncertain reliability. By mid-May, an elastic FEM model was produced, but more for the purpose of exploring ground displacement patterns from a pressurized intrusion than for direct evaluation of stability (Ewart & Voight 1980). However, the serious anticipation of a very large slope failure was not a view held unanimously; there was not 'institutional consensus' among the scientists assembled (Voight 1988). Among outcomes preferred by some scientists was the breakout of a north-flank lava dome, or a north-flank landslip much smaller than that which occurred on 18 May.

Without short-term warning or change in deformation rate, but accompanied and probably triggered by a magnitude 5.2 earthquake, the north flank collapsed in a sequence of slope failures on 18 May 1980 (Voight 1981). In turn, the decompressions associated with sequential slope movements resulted in multiple magmatic and hydrothermal explosions that generated a complex, northward-directed volcanic blast (Hoblitt, this issue). The failed edifice mass had a volume of *ca.* $2.3\ \mathrm{km}^3$, and generated an avalanche deposit of $2.8\ \mathrm{km}^3$ (Voight *et al.* 1981; Glicken 1986). Some
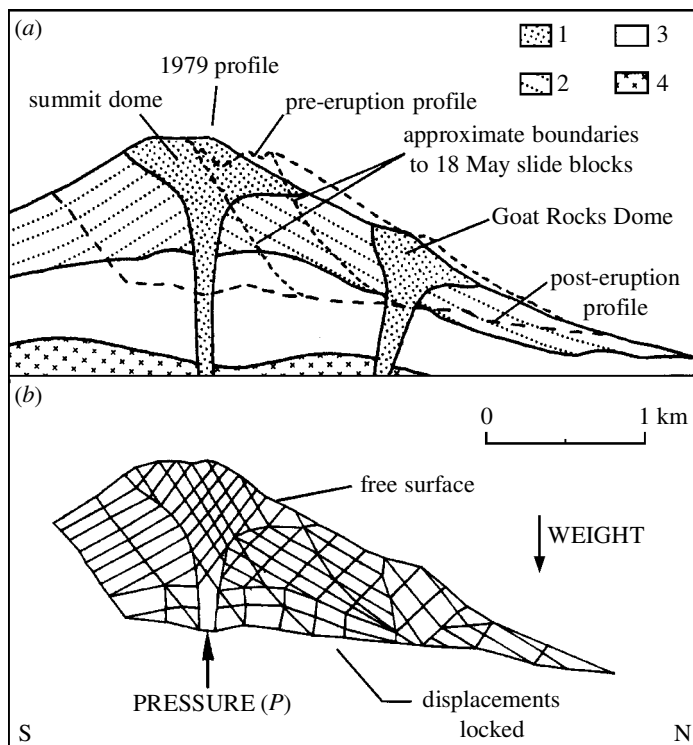
Figure 5. Cross-section of Mt St Helens showing (*a*) pre-eruption and post-eruption profiles and slide blocks of 18 May 1980. (1) Dacite domes, more than 200 years old. (2) Modern cone with lava flows and fragmental material. (3) Older dacite dome complex with fragmental material. (4) Tertiary bedrock (after Voight *et al.* 1981). (*b*) Numerical block model, with weight of material applied. Magma pressure is then applied to central conduit (after Paul *et al.* 1987).

materials testing was carried out, and hindcast stability analyses of the failure were carried out by Voight *et al.* (1983), using (mainly) the two-dimensional modified Bishop procedure for circular slip surfaces, and other methods for trial surfaces of irregular shape. The results suggested that high pore-water pressures and earthquake shaking were required to destabilize the edifice, in conjunction with the disruption and other effects caused by shallow magmatic intrusion.

Subsequently, the slope was evaluated by Paul *et al.* (1987) using a numerical model comprising a two-dimensional assemblage of rigid blocks deforming in plain strain (Pouyet *et al.* 1983). Pore-fluid pressure was not taken into account, but the model was otherwise sophisticated and showed that the loading resulting from intruding magma was able to cause the precursory surface deformations observed (figures 5 and 6). The authors confirm that the gravitational failure was due to cumulative factors, including magmatic pressure, and a trigger earthquake. Numerical modelling enabled a much-improved understanding of the process.

The lack of accelerated creep prior to slope collapse was considered by Voight (1988), who suggested calculation of rupture life t_f in terms of steady state creep rate, in simplified form $t_f = 214\xi^{-1}$ (± 0.59), where t_f is in minutes from inception of loading, and ξ is the creep rate in units of $10^{-4}\,\mathrm{min}^{-1}$. The equation suggests
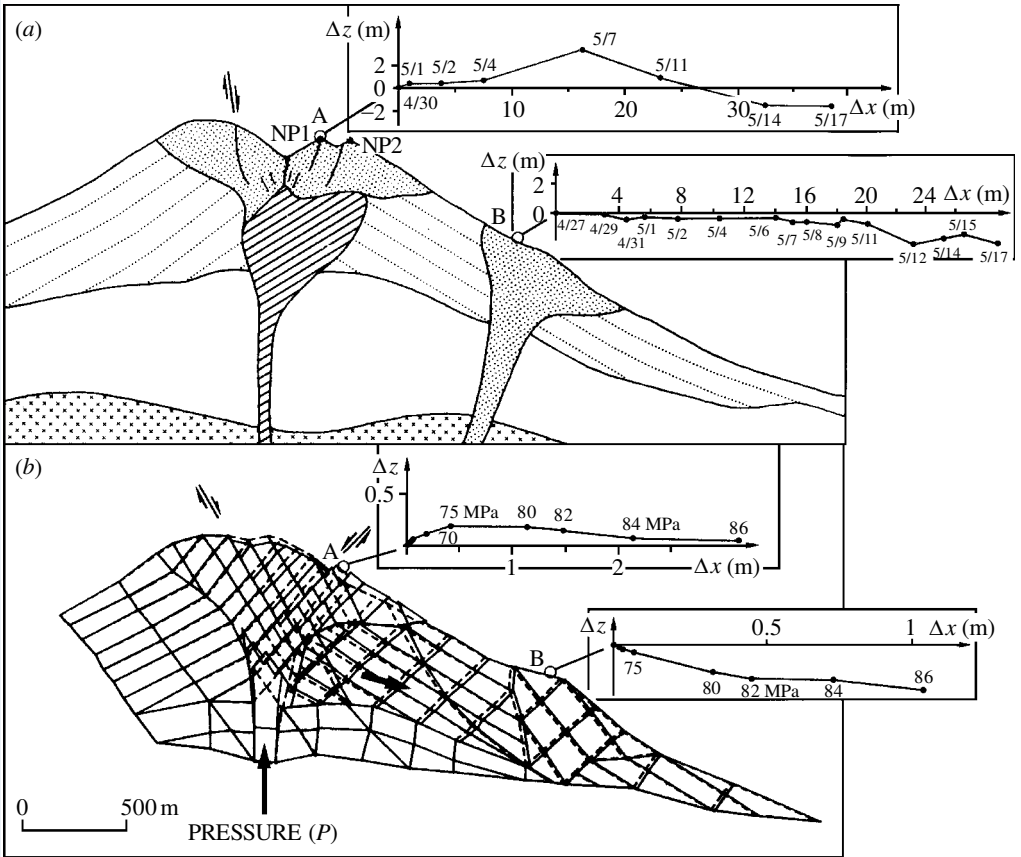
Figure 6. Cross-sections of Mt St Helens, comparing (*a*) displacements observed at North Point (point A) and Goat Rocks (point B) (after Lipman *et al*. 1981; Moore & Albee 1981) with (*b*) those generated by simulation (multiplied by 20), for an internal pressure of 86 MPa in the block-deformation model. Deformed grid, solid lines; initial state, dashed lines (after Paul *et al*. 1987).

a rupture window at Mt St Helens of 5–82 days, which encloses the 18 May 1980 collapse, for which t_f was 53 days. The confidence limits are large, but the relation's importance is to emphasize the inevitability of sector failure within weeks, if continued forcible magma emplacement causes high rates of edifice strain and localized shearing.

More recently, numerical dynamic modelling of the sequential failure and debris avalanche emplacement was presented by Sousa & Voight (1991, 1995); Donnadieu & Merle (1998) discussed scaled physical models of the deformation produced by a rising intrusion at Mt St Helens; and Reid *et al*. (2000) use the 1980 Mt St Helens slope to test a three-dimensional LEA model (with spherical failure surfaces) in conjunction with digitized topography (DEM). The latter study confirmed the viability of the LEA method to search a DEM, to recognize potentially unstable areas of the edifice and the associated failure volumes. The Donnadieu–Merle study demonstrated that viscous injections could create a curved major shear and a bulging flank, similar in many respects to that observed at Mt St Helens.
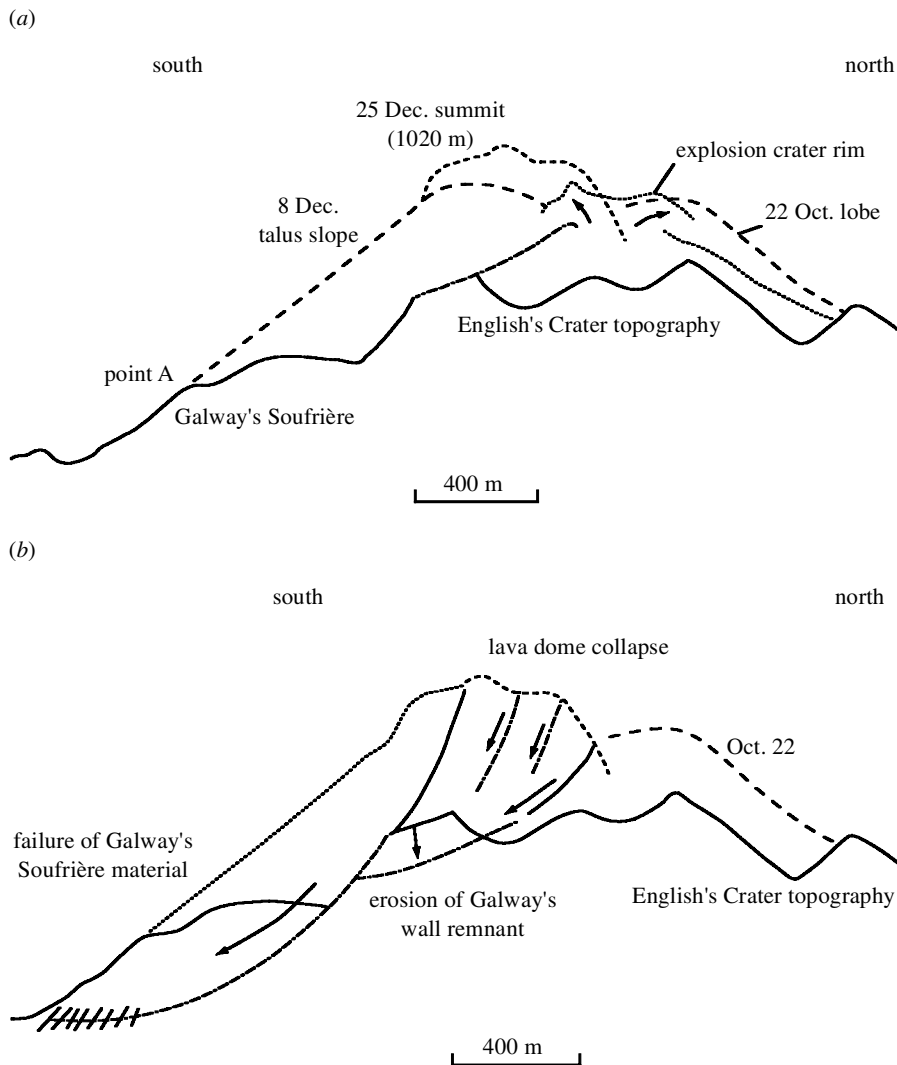
(*a*)

(*b*)

Figure 7. Cross-sections through Soufrière Hills volcano before (*a*) and after (*b*) the 26 December 1997 collapse. The pre-eruption conditions included English's Crater and Galway's Soufrière. Additional materials comprise lavas and talus. In (*b*), the collapse first involved new dome lava and talus, and underlying Soufrière material, followed by explosive collapse of decompressed fresh dome lavas.

(*b*) *Stability of Soufrière Hills volcano, December 1997*

To paraphrase Lord Beveridge, 'Montserrat was not only a natural laboratory for mixing magmas, but a laboratory for mixing scientists', and, in both instances, the results could be explosive. The growth (since 1995) of an andesite lava dome at Soufrière Hills caused instability of the southern flank of the volcano. The region of failure included hydrothermally altered rock and active fumaroles. Indications of potential instability were recognized as early as October 1996, but catastrophic failure occurred at night, during a period of enhanced seismicity, on 26 December 1997

(Sparks *et al.* 2000). In the two months before the failure, the lava dome and talus apron had grown rapidly outward over the hydrothermally weakened area (figure 7*a*). The failure in December generated a debris avalanche with a volume of 50×10^6 m^3, and about 30×10^6 m^3 of the pressurized lava dome then disintegrated to generate a high-energy pyroclastic density current that devastated 10 km^2 of southern Montserrat (figure 7*b*; see also Sparks *et al.* (2000) and Ritchie *et al.* (2000)). There was no loss of life, because the area had been evacuated when the signs of potential instability of the south flank were recognized in late 1996.

Unlike Mt St Helens, preliminary quantitative stability assessments using two-dimensional LEA were used by Voight during hazards assessments at Soufrière Hills in March and December 1996. Block samples of indurated volcanic breccias and dome rock were collected in early 1996 from crater-wall areas, including the south flank area later buried by rockfall debris and dome talus. The samples were tested for stress–strain behaviour and strength under triaxial loading conditions, tensile strength and bulk density, and samples of unconsolidated debris were tested in direct shear (Voight 1996). The test data, evaluated in terms of Mohr–Coulomb and Hoek–Brown parameters, were used to constrain the stability analyses; scaled reductions were used for rock-mass properties.

Additionally, two-dimensional (axisymmetric) elastic homogeneous FEMs were conducted to explore the stress changes associated with dome growth and internal pressurization for the geometry existing in late 1996 (Wadge *et al.* 1998). The analysis was limited inasmuch as pore pressures, seismic loading, material zonation and plastic deformation were not treated. Relative stability was interpreted from the ratios of elastic shear stresses to an assumed Coulomb relation.

LEA analyses were also carried out by Voight in January 1998, soon after the failure, and some additional sampling and testing was conducted. However, all the modelling referred to above was limited in that stress–strain behaviour, development of plastic zones and strength weakening, and dynamic loading, among other aspects, could not be adequately represented. Preferably, the *mechanism* of failure should be elucidated by modelled strain localizations, rather than be pre-specified, as in LEA modelling, or vaguely interpreted from elastic FEM. What triggered the failure? Was it seismic shaking? Conduit pressure? Forcible emplacement of a new lobe of lava?

The results of a series of two-dimensional explicit plain-strain FDM models of the Soufrière Hills slope are presented to illustrate this question. The slope is subdivided into four zones, representing (1) fresh dome talus, (2) fresh lava, (3) altered Soufrière material, (4) old edifice (as shown in figure 8*a*), with the actual material parameter values different in various models. In general, bulk modulus is taken as 20 GPa and shear modulus is 10 GPa. The models undergo plastic deformation when Coulomb yield limits, different in the various zones, are reached. In some cases, pseudo-static loads simulate earthquake loading. Figure 8*a* shows assumed material zonation and shear strain-rate contours for the slope subjected to seismic loading, with figure 8*b* also showing displacement–velocity vectors. The velocity and strain fields are more-or-less consistent with the position of the actual failure surface 'observed' at Montserrat, and suggests that strong seismic shaking may possibly be a viable trigger to slope failure.

The lava-lobe emplacement model is shown in figure 9*a, b*, whereby lava in the upper part of the slope is squeezed southwards at a constant rate, creating a shear zone that extends to the toe of the slope and includes altered Soufrière material
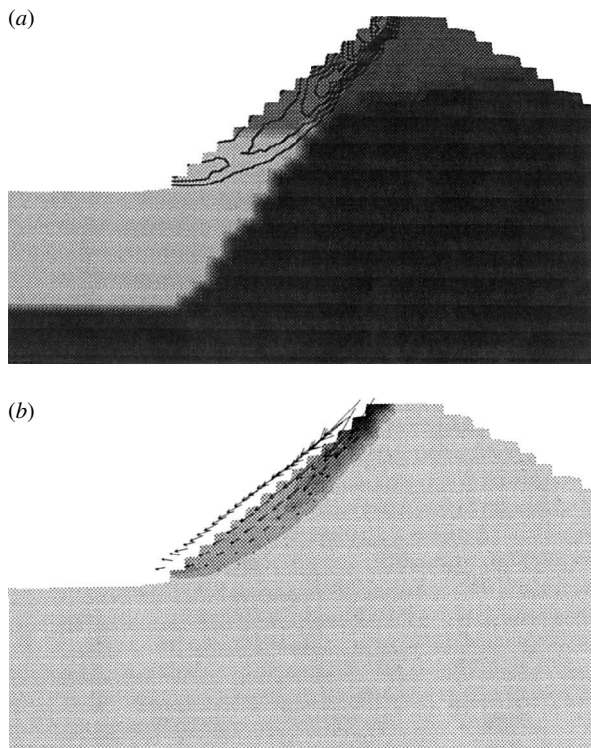
Figure 8. Numerical model of the Soufrière Hills volcano, zoned in (a) to show: (1) fresh dome talus (medium grey, under contours on upper slope); (2) fresh lava (dark grey, upper part of volcano); (3) altered Soufrière materials (pale grey); (4) old edifice materials. Failure indicated by shear strain-rate contours. Coulomb parameters in zone 1 are $c' = 10$ kPa, $\phi' = 40°$; in zone 3 they are $c' = 50$ kPa, $\phi' = 40°$. Seismic loading coefficient $= 0.15g$. (b) Same as (a) but with zero seismic loading. Shear strain rate, shading, with velocity vectors (maximum of 0.037 m s^{-1}).

(see the velocity field in figure 9b). As a consequence of this deformation, material in zones 1 and 3, as defined above, are assumed to strain weaken, with the result that gravitational collapse occurs in the outer slope (figure 10a) at rates that exceed the continuing lava-lobe emplacement (figure 10b). Next, the gravity collapse of the outer part of the slope results in an oversteepened and decompressed face of fresh lava, which begins to collapse explosively (figure 10c) to generate a volcanic blast, the details of which are beyond the scope of the model. In general, the models support the plausibility of the lava-lobe-emplacement collapse mechanism.

Conduit pressure can also be modelled, although these pressures dissipate radially, and a two-dimensional model only provides an upper bound to the stresses. On balance, the analyses favour collapse resulting from rapid forcible lava-lobe emplacement, and gravity slip-surface localization with strain weakening, probably also influenced by seismic shaking.

(c) *Lava spines at Lamington, Papua New Guinea, and Mont Pelée, Martinique*

In November 1902, after the catastrophic eruptions of 1902 at Mont Pelée, a great spine of lava rose above the crater.
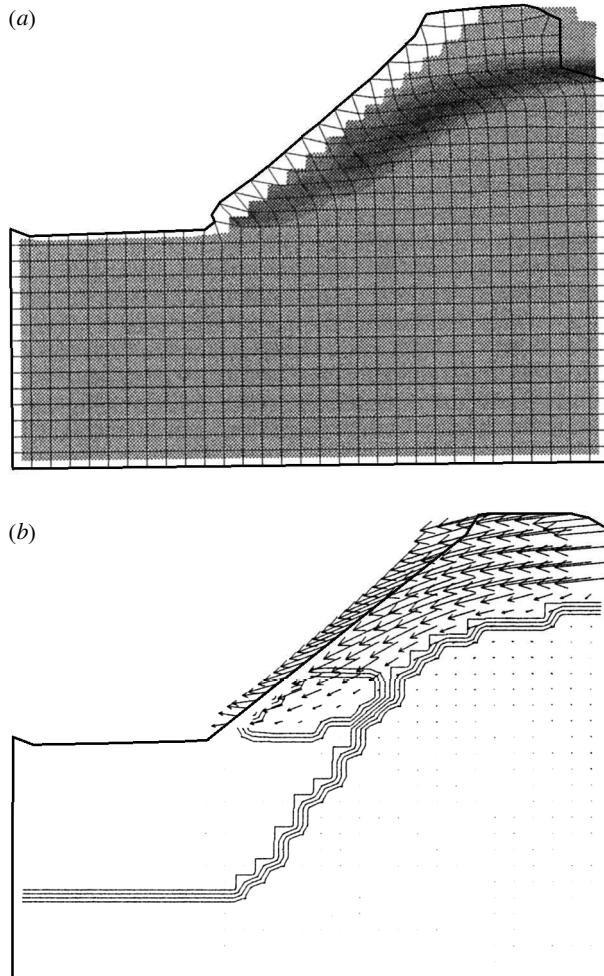
Figure 9. Numerical model of lava-lobe emplacement at Soufrière Hills. Lava in the upper part
of the slope is pushed southwards at a constant rate to create a shear zone that extends to
the toe of the slope and includes altered Soufrière material (see the velocity field in figure 9b).
(a) Deformed grid and shear strain rate, shading. Grid distortion scale 190 times. (b) Material
zonation (simplified from figure 8) and velocity vectors (maximum of 0.65 m s^{-1}). The zone at
the toe of slope is Soufrière material susceptible to strain weakening.

> Growing at about 10 metres a day, by May 1903 the spine was no less
> than 310 metres high, rearing above St Pierre like an obelisk, a memorial
> to the thousands that had died below   (Francis 1993).

Following the great 1951 eruption of Lamington, a typical Peléean dome grew to a
height of 600 m and exhibited numerous spines, one of which grew to 100 m high at a
rate of 1 m d^{-1} (Taylor 1958). Spines of similar size and growth rates have occurred
on Montserrat. Like those of Pelée, many exhibited a 'half-horn' shape, 'one side
smoothly curved and lineated during extrusion like wire through a die, the other
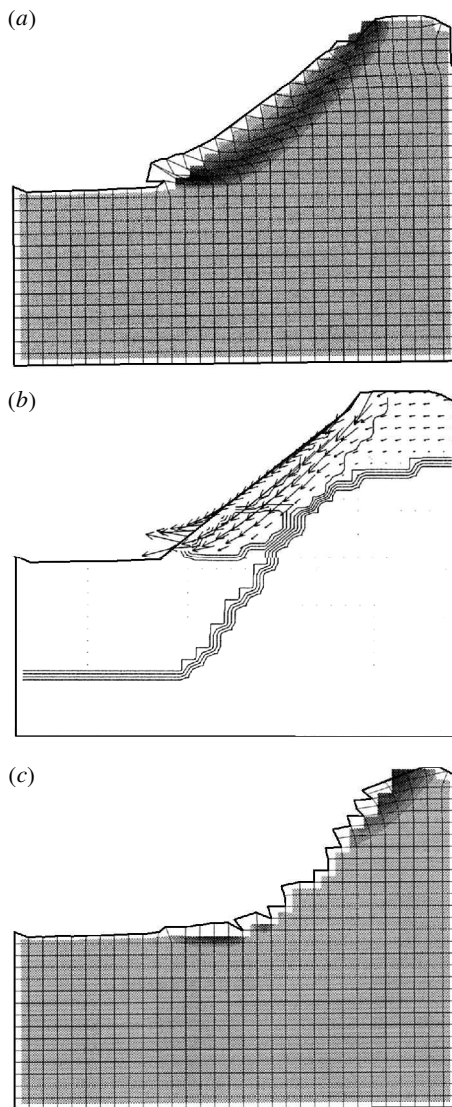jagged and fractured' (Francis 1993; cf. Lacroix 1904).

B. Voight

(a)

(b)

(c)

Figure 10. As figure 9, with material strain-weakened to $c' = 20$ kPa, $\phi' = 30°$, zone 1 (talus), and $c' = 20$ kPa, $\phi' = 20°$, zone 3 (Soufrière). Lava-lobe emplacement continues, but gravity movement on outer slope dominates the grid distortion (a) and velocity vector field (b). Grid distortion scale 24 times, maximum vector 5.0 m s^{-1}. (c) Gravity collapse of the outer part of the slope results in an oversteepened and decompressed face of fresh lava, which begins to collapse explosively (grid distortion scale 1.1 times). Generation of the volcanic blast is beyond the scope of the model.

The height of the spine is partly controlled by the extrusion pressure, which is countered by the increasing back pressure associated with the weight of the growing spine. The height achieved can also be influenced by material strength, for, as the spines rise, the stresses near their exposed base increase. If these stresses reach critical values, the spine will collapse, as illustrated by two-dimensional analysis in figure 11
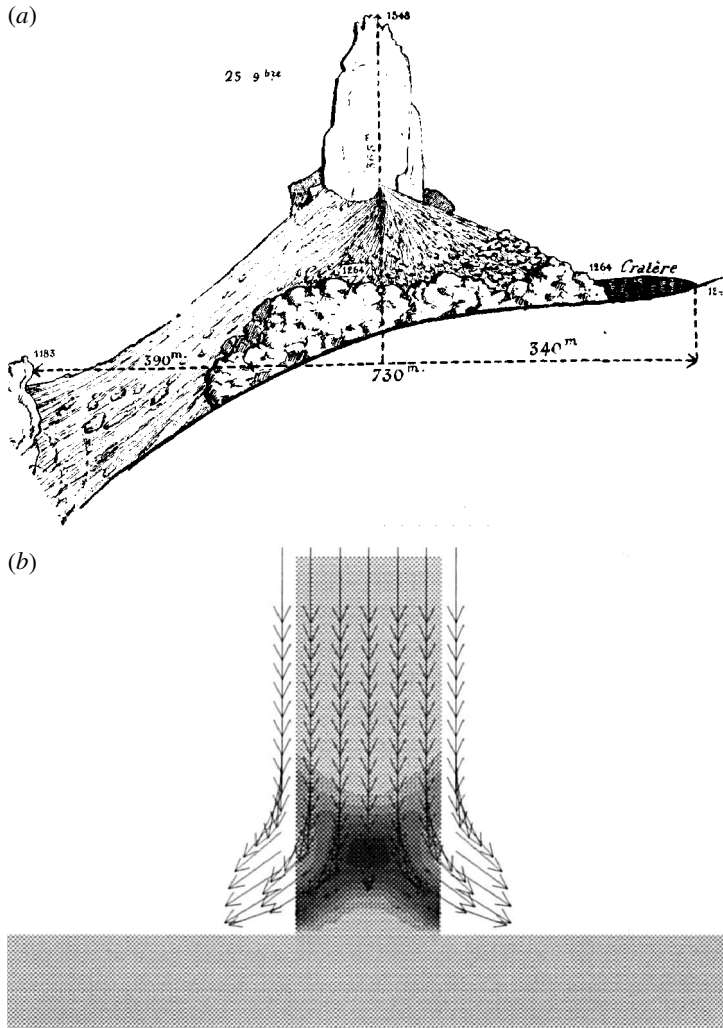
Figure 11. (*a*) Lava spine at Mont Pelée on 25 November 1902 (after Lacroix 1904). (*b*) Numerical model of a cohesive lava spine 100 m high and 46 m broad. If spine height and stresses reach critical values, the spine will collapse.

for a purely cohesive spine 100 m high and 46 m broad. In this sense, the spines may be considered to have a theoretical *critical height*, which, if exceeded, will result in failure. In reality, the concept is more complex, as the mass strength continuously varies due to cooling, degassing, fracturing and rain-water infiltration, is a function of growth rate, spine shape and other factors, and is heterogeneously distributed over the volume of the spine. Moreover, the strength and creep properties of highly crystalline hot lava are still poorly understood.

(*d*) *Retrogressive lava-dome collapses, Montserrat*

The stability of growing domes has much in common with edifice collapse, and distinctions between the two phenomena can become blurred in comparing growing
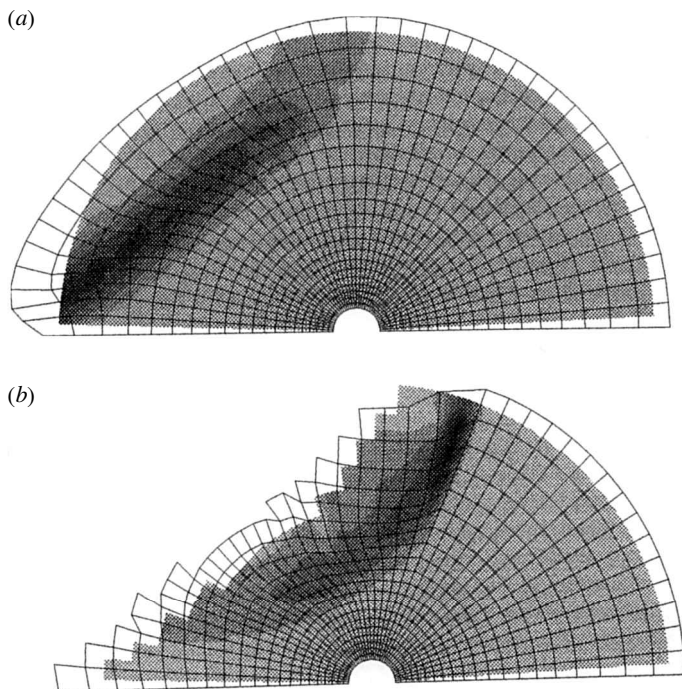
(*a*)

(*b*)

Figure 12. Numerical model (two dimensional) of a lava dome. (*a*) When the dome interior is critically stressed (by increased size, or oversteepening) or weakened (e.g. by fresh injected magma, or fractured carapace), gravitational failure can initiate, as indicated by the shear strain-rate contours. In the case shown, left-side weakness promotes single-side failure. With removal of failed material (*b*) a new failure zone develops. Successive failures can promote depressurization and spontaneous disintegration of dome core material.

domes to edifices with intruding silicic magma. Major collapses of the lava dome of Soufrière Hills volcano occurred on 17 September 1996, and 25 June, 3 August and 21 September 1997 (Robertson *et al.* 1998; Young *et al.* 1998), triggering explosive eruptions. The collapses occurred in a retrogressive fashion over a period of several hours, with successive collapses excavating deep into the dome interior (figures 12–14). The situation is simulated by the generalized two-dimensional analysis of a lava dome (figure 12). When the dome interior is critically stressed (by increased size, or oversteepening) or weakened (e.g. by fresh injected magma, or fractured carapace), gravitational failure can be initiated, as indicated by the shear strain-rate contours. Spontaneous disintegration of the detached mass by decompressed diffused and vesicular volatiles may then lead to gas-fluidized dense particulate (block-and-ash) flows and/or transport of dispersed finer particles in an expanding gaseous surge (Fink & Kieffer 1993; Alidibirov & Dingwell 1996). However, the remaining cavity walls are often unstable, and a second collapse may then occur (figure 12*b*). Pressurized vesicles may be considered as micro-scale weakening mechanisms within the bulk lava, decreasing its strength and mass stability. Successive collapses in this fashion may lead to a series of pyroclastic flows, and to conduit decompression that results in vertical explosions (see, for example, Newhall & Melson 1987; Sato *et al.* 1992).
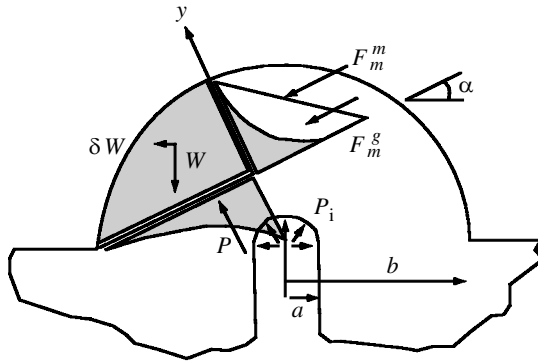
Figure 13. Section through a dome subject to gas pressure P_i in internal cavity. The diffusive gas pressure acts on the basal (P) or rear boundaries (F_m^g) of a failing block of mass W and seismic loading δ. Magmastatic pressure potentially at block rear is F_m^m (after Voight & Elsworth 2000).

Figure 14. Glowing andesite lava dome at Soufrière Hills volcano, Montserrat, West Indies, in January 1997. Substantial evidence supports internal gas pressurization of the dome and upper conduit. Lava temperature in dome core about 800 °C. Dome is enveloped in ash and gas emitted by dome, and wrapped against the dome by prevailing easterly winds. The strong winds influence the dynamics of pyroclastic currents generated by dome collapse.

Gas overpressures can influence the failure process. Voight & Elsworth (2000) develop diffusion models to calculate gas overpressures in a lava dome (Carslaw & Jaeger 1959), and embed these data in stability analyses to demonstrate that gas pressurization can initiate deep-seated instability (figures 13 and 14). Tilt data indicate that conduit pressurization on Montserrat oscillated, and that a number of oscillations (as many as nine) may have occurred before failure initiated (Voight *et al.* 1998, 1999). This result suggests that in some cases a number of gas-pressure oscillations over a period of time may be required for failure, with the timing of potential failure influenced by the migration velocity of the pressure pulse from the dome core. The time to failure is conditioned by hydraulic/gas diffusivity, with values of the order of $1000 \text{ m}^2 \text{ s}^{-1}$ capable of sustaining failure for magnitudes of overpressure approaching 10 MPa. Results presented by Voight & Elsworth (2000) are consistent with observed lava-dome failures on Montserrat, hours to days after the onset of pressurization. The need for these large gas pressures is eased for a weaker dome, fatigue weakening of the dome with cyclic pressurization, or with augmenting earthquake loads. A viable alternative hypothesis is weakening of a heterogeneous dome, and local oversteepening, by repeated vigorous injections of volatile-rich magma.

References

Alidibirov, M. & Dingwell, D. B. 1996 Magma fragmentation by rapid decompression. *Nature* **380**, 146–148.

Alidibirov, M., Dingwell, D. B., Stevenson, R. J., Hess, K.-U., Webb, S. L. & Zinke, J. 1997 Physical properties of the 1980 Mount St Helens cryptodome magma. *Bull. Volcanol.* **59**, 103–111.

Barton, N. R. & Bandis, S. C. 1982 Effects of block size on the shear behaviour of jointed rock. In *23rd US Symp. Rock Mechanics*, pp. 739–760.

Barton, N. R. & Bandis, S. C. 1990 Review of predictive capabilities of JRC-JCS model in engineering practice. In *Proc. Int. Symp. Rock Joints* (ed. N. Barton & O. Stephansson), pp. 603–610. Rotterdam: Balkema.

Beget, J. & Kienle, J. 1992 Cyclic formation of debris avalanches at Mount St Augustine volcano. *Nature* **356**, 701–704.

Belousov, A. B. 1995 The Shiveluch volcanic eruption of 12 November 1964: explosive eruption provoked by failure of the edifice. *J. Volcanol. Geotherm. Res.* **66**, 357–365.

Belousov, A. B., Belousova, M. & Voight, B. 1999 Multiple edifice failures, debris avalanches, and associated eruptions in the Holocene history of Shiveluch volcano, Kamchatka, Russia. *Bull. Volcanol.* **61**, 324–342

Bieniawski, Z. T. 1989 *Engineering rock mass classifications.* Wiley.

Bishop, A. W. 1955 The use of the slip circle in the stability analysis of slopes. *Géotechnique* **5**, 7–17.

Brown, C. B. & King, I. P. 1966 Automatic embankment analysis: equilibrium and stability conditions. *Géotechnique* **16**, 209–219.

Byrne, P. M., Jitno, H. & Salgado, R. 1992 Earthquake-induced displacements of soil-structure systems. In *Proc. 10th World Conf. Earthquake Engng, Madrid*, vol. 3, pp. 1407–1412.

Carslaw, H. S. & Jaeger, J. C. 1959 *Conduction of heat in solids*, 2nd edn. Oxford University Press.

Cundall, P. A. 1980 UDEC—a generalized distinct element program for modeling jointed rock. US Army, Contract DAJA37–79-C-0548; NTIS no. AD-A087–610/2.

Cundall, P. A. 1990 Numerical modeling of jointed and faulted rock. In *Mechanics of jointed and faulted rock*, pp. 11–18. Rotterdam: Balkema.

Cundall, P. A. & Board, M. 1988 A microcomputer program for modeling large-strain plasticity problems. In *Numerical methods in geomechanics* (ed. G. Swoboda). pp. 2101–2108. Rotterdam: Balkema.

Dade W. B. & Huppert, H. E. 1998 Long-runout rockfalls. *Geology* **26**, 803–806.

Decker, R. W. 1981 The 1980 activity: a case study in volcanic eruption forecasting. *Prof. Paper US Geol. Surv.* **1250**, 815–820.

Desai, C. S. & Abel, J. F. 1972 *Introduction to the finite element method*. New York: Van Nostrand.

De Silva, S. L. & Francis, P. W. 1991 *Volcanoes of the Central Andes*. Springer.

Dingwell, D. B. 1998 Recent experimental progress in the physical description of silicic magma relevant to explosive volcanism. In *The physics of explosive volcanism* (ed. J. S. Gilbert & R. J. S. Sparks), vol. 145, pp. 9–26. London: Geological Society.

Donnadieu, F. & Merle, O. 1998 Experiments on the indentation process during cryptodome intrusions: new insights into Mount St Helens deformation. *Geology* **26**, 79–82.

Drescher, A. & Mroz, Z. 1997 A refined superior sand model. *Proc. 6th Int. Symp. Num. Models Geomech., NUMOG 6*, pp. 21–26. Balkema: Rotterdam.

Duncan, J. M. 1992 State-of-the-art: static stability and deformation analysis. *Am. Soc. Civil Engng Geotech.* (Spec. Publ.) **31**, 222–265.

Duncan, J. M. 1996 State-of-the-art: limit equilibrium and finite-element analysis of slopes. *J. Geotech. Engng ASCE* **122**, 577–596.

Duncan, J. M. & Wright, S. G. 1980 The accuracy of equilibrium methods of slope stability analysis. *Eng. Geol.* **16**, 5–17.

Elsworth, D. & Voight, B. 1995 Dike intrusion as a trigger for large earthquakes and the failure of volcano flanks. *J. Geophys. Res.* **100**, 6005–6024.

Ewart, J. & Voight, B. 1980 Finite element deformation models, Mount St Helens volcano, Washington: preliminary results. Technical report to US Geological Survey, Investigation for Mount St Helens Eruption. File report: Cascades Volcano Observatory, Washington (report summary submitted by letter to USGS, 16 May 1980).

Fink, J. H. & Kieffer, S. W. 1993 Estimates of pyroclastic flow velocities resulting from explosive disintegration of lava domes. *Nature* **363**, 612–614.

Finn, W. D. L. 1988 Dynamic analysis in geotechnical engineering. *Geotech. ASCE* (Spec. Publ.) **20**, 523–591.

Finn, W. D. L., Yogendrakumar, M., Yoshida, M. & Yoshida, N. 1986 *TARA-3: a program to compute the response of 2-D embankments and soil-structure interaction systems to seismic loadings*. Vancouver: University of British Columbia.

Francis, P. W. 1993 *Volcanoes: a planetary perspective*. Oxford: Clarendon.

Francis, P. W. & Self, S. 1987 Collapsing volcanoes. *Sci. Am.* **287**, 90–99.

Francis, P. W. & Wells, G. L. 1988 Landslide thematic mapper observations of debris avalanche deposits in the Central Andes. *Bull. Volcanol.* **50**, 258–278.

Francis, P. W., Gardeweg, M., Ramirez, C. F. & Rothery, D. A. 1985 Catastrophic debris avalanche deposit of Socompa volcano, northern Chile. *Geology* **13**, 600–603.

Fredlund, D. G. 1984 Analytical methods for slope stability analysis. *Proc. 4th Int. Symp. Landslides, Toronto*, vol. 1, pp. 229–250.

Glicken, H. 1986 Rockslide-debris avalanche of May 18, 1980, Mount St Helens volcano, Washington. PhD thesis, University of California, Santa Barbara.

Goodman, R., Taylor, R. & Brekke, T. 1968 A model for the mechanics of jointed rock. *J. Soil Mech. Found. Div. ASCE* **94**, 637–659.

Gorshkov, G. S. 1959 Gigantic eruption of the volcano Bezymianny. *Bull. Volcanol.* **21**, 77–109.

Hart, R. D., Cundall, P. A. & Lemos, J. 1988 Formulation of a three dimensional distinct element model. Part II. Mechanical calculations of motion and interaction of a system composed of many polyhedral blocks. *Int. J. Rock Mech. Min. Sci.* **25**, 117–126.

Hess, K.-U. & Dingwell, D. B. 1996 Viscous hydrous leucogranite melts: a non-Arrhenian model. *Am. Min.* **81**, 1297–1301.

Hoek, E. 1983 Strength of jointed rock masses. *Géotechnique* **33**, 187–223.

Hoek, E. & Brown, E. T. 1980 Empirical strength criterion for rock masses. *J. Geotech. Engng Div. ASCE* **106**, 1013–1035.

Hoek, E. & Brown, E. T. 1988 The Hoek–Brown failure criterion—a 1988 update. *Proc. 15th Canadian Rock Mech. Symp, Toronto*.

Hoek, E., Wood, D. & Shah, S. 1992 A modified Hoek–Brown criterion for jointed rock masses. *Int. Symp. Soc. Rock Mech., Eurock '92*, pp. 209–214. London: British Geological Society.

Hoek, E., Kaiser, P. K. & Bawden, W. F. 1994 *Support of underground excavations in hard rock*. Rotterdam: Balkema.

Hungr, O. 1987 An extension of Bishop's simplified method of slope stability analysis to three dimensions. *Géotechnique* **37**, 113–117.

Hungr, O., Salgado, F. M. & Byrne, P. M. 1989 Evaluation of a three dimensional method of slope stability analysis. *Can. Geotech. J.* **26**, 679–686.

Iverson, R. M. 1995 Can magma-injection and groundwater forces cause massive landslides on Hawaiian volcanoes? *J. Volcanol. Geotherm. Res.* **66**, 295–308.

Johnson, R. W. 1987 1888 slope failure of Ritter volcano: results from a bathymetric survey, and examples from other Papua New Guinea volcanoes. *Bull. Volcanol.* **49**, 669–679.

Kienle, J., Kowalik, Z. & Murty, T. S. 1987 Tsunamis generated by eruptions from St Augustine volcano, Alaska. *Science* **236**, 1445–1447.

Lacroix, A. 1904 *La Montagne Pelée et ses éruptions*. Paris: Masson.

Lipman, P. W. & Mullineaux, D. R. (eds) 1981 The 1980 eruptions of Mount St Helens, Washington. *Prof. Paper US Geol. Surv.* **1250**.

Lipman, P. W., Moore, J. G. & Swanson, D. A. 1981 Bulging of the north flank before the May 18 eruption: geodetic data. *Prof. Paper US Geol. Surv.* **1250**, 143–156.

McGuire, W. J., Kilburn, C. R. & Murray, J. 1995 *Monitoring active volcanoes: strategies, procedures and techniques*. London: UCL Press.

Miller, C. D., Mullineaux, D. R. & Crandell, D. R. 1981 Use of volcanic hazards assessments: a case study at an active volcano. *Prof. Paper US Geol. Surv.* **1250**, 789–802.

Moore, J. G. & Albee, W. C. 1981 Topographic and structural changes, March–July 1980: photogrammatic data. *Prof. Paper US Geol. Surv.* **1250**, 123–134.

Morgenstern, N. R. 1992 The evaluation of slope stability—a 25-year perspective. *Am. Soc. Civil Engng Geotech.* (Spec. Publ.) **31**, 1–26.

Murray, J. B., Voight, B. & Glot, J.-P. 1994 Slope movement crisis on the east flank of Mt Etna volcano: models for eruption triggering and forecasting. *Engng Geol.* **38**, 245–259.

Mustoe, G. (ed.) 1989 *Proc. 1st US Conf. Discrete Element Methods*. Golden, CO: Colorado School of Mines.

Naranjo, J. & Francis, P. W. 1987 High velocity debris avalanche at Lastarria volcano, north Chile. *Bull. Volcanol.* **49**, 509–514.

Nash, D. F. T. 1987 A comparative review of limit equilibrium methods of stability analysis. In *Slope stability* (ed. M. G. Anderson & K. S. Richards), ch. 2. Wiley.

Newhall, C. G. & Melson, W. G. 1987 Explosive activity associated with growth of volcanic domes. *J. Volcanol. Geotherm. Res.* **17**, 111–131.

Okada, H. 1983 Comparative study of earthquake swarms associated with major volcanic activities. In *Arc volcanism: physics and tectonics* (ed. D. Shimozuro & I. Yokoyama), pp. 43–61. Tokyo: Terra Science.

Oyagi, N. 1987 The 1984 Ontake-san landslide and its movement. *Trans. Jap. Geomorphol. Un.* **8**, 127–144.

Pariseau, W. G. & Voight, B. 1979 Rockslides and avalanches: basic principles and perspectives in the realm of civil and mining operations. In *Rockslides and avalanches, 2: engineering sites* (ed. B. Voight), pp. 1–92. Amsterdam: Elsevier.

Pariseau, W. G., Voight, B. & Dahl, H. D. 1970 Finite element analyses of elastic-plastic problems in the mechanics of geologic media. *Proc. 2nd Int. Congr. Soc. Rock Mech., Beograd*, paper 3-45.

Paul, A., Gratier, J. P. & Boudon, J. 1987 A numerical model for simulating deformation of Mount St Helens volcano. *J. Geophys. Res.* **92**, 10 299–10 312.

Pietruszczak, S. & Mroz, Z. 1981 Finite element analysis of deformation of strain-softening materials. *Int. J. Num. Meth. Engng* **17**, 327–334.

Pouyet, P., Picaut, J., Costaz, J. L. & Dulac, J. 1983 'Bloc' program for elasto-plastic calculations of fissured media. In *Proc. 7th Structural Mechanics Reactor Technology, Chicago*.

Reid, M. E., Christian, S. & Brien, D. L. 2000 Gravitational stability of three-dimensional stratovolcanic edifices. *J. Geophys. Res.* **105**, 6043–6056.

Ritchie, L. J., Cole, P. & Sparks, R. S. J. 2000 Sedimentology of the pyroclastic density current deposits generated by the December 26, 1997 eruption at the Soufrière Hills volcano, Montserrat. *Geol. Soc.* (Spec. Publ.). (In the press.)

Robertson, R. (and 10 others) 1998 The explosive eruption of Soufrière Hills volcano, Montserrat, West Indies, September 17, 1996. *Geophys. Res. Lett.* **25**, 3429–3433.

Sarma, S. K. 1979 Stability analysis of embankments and slopes. *J. Geotech. Engng Div. ASCE* **105**, 1511–1524.

Sato, H., Fujii, T. & Nakada, S. 1992 Crumbling of dacite dome lava and generation of pyroclastic flows at Unzen volcano. *Nature* **360**, 664–666.

Scarpa, R. & Tilling, R. I. 1996 *Monitoring and mitigation of volcanic hazards.* Springer.

Seed, H. B. 1979 Considerations in the earthquake-resistant design of earth and rockfill dams. *Géotechnique* **29**, 215–263.

Sekiya, S. & Kikuchi, Y. 1889. The eruption of Bandai-san. *Tokyo Imp. Univ. Coll. Sci. J.* **3**, 91–172.

Shah, S. 1992 A study of the behaviour of jointed rock masses. PhD thesis, University of Toronto.

Siebert, L. 1984 Large volcanic debris avalanches: characteristics of source areas, deposits, and associated eruptions. *J. Volcanol. Geotherm. Res.* **22**, 163–197.

Siebert, L. 1996 Hazards of large volcanic debris avalanches and associated eruptive phenomena. In *Monitoring and mitigation of volcano hazards* (ed. R. Scarpa & R. I. Tilling), pp. 541–572. Springer.

Siebert, L., Glicken, H. & Ui, T. 1987 Volcanic hazards from Bezymianny- and Bandai-type eruptions. *Bull. Volcanol.* **49**, 435–459.

Siebert, L., Beget, J. E. & Glicken, H. 1995 The 1883 and late prehistoric eruptions of Augustine volcano, Alaska. *J. Volcanol. Geotherm. Res.* **66**, 367–395.

Sleep, N. H. 1999 Rate- and state-dependent friction of intact rock and gouge. *J. Geophys. Res.* **104**, 17 847–17 855.

Slingerland, R. L. & Voight, B. 1979 Occurrences, properties, and predictive models of landslide-generated water waves. In *Rockslides and avalanches, 2: engineering sites* (ed. B. Voight), pp. 317–397. Amsterdam: Elsevier.

Sousa, J. & Voight, B. 1991 Continuum simulation of flow failure. *Géotechnique* **41**, 515–538.

Sousa, J. & Voight, B. 1995 Multiple-pulsed debris avalanche emplacement at Mount St Helens in 1980: evidence from numerical continuum flow simulation. *J. Volcanol. Geotherm. Res.* **66**, 227–250.

Sparks, R. S. J. (and 11 others) 2000 Generation of a debris avalanche and violent pyroclastic density current: the Boxing Day eruption of 26 December 1997 at the Soufrière Hills volcano, Montserrat. *Geol. Soc.* (Spec. Publ.). (In the press.)

Spencer, E. 1981 Slip circles and critical shear planes. *J. Geotech. Engng Div. ASCE* **107**, 929–942.

Starfield, A. M. & Cundall, P. A. 1988 Towards a methodology for rock mechanics modeling. *Int. J. Rock Mech. Min. Sci. Geomech. Abs.* **25**, 99–106.

Succarieh, M. F., Yan, L. & Elgamal, A. M. 1991 Modelling of observed deformation at La Villita dam. *Proc. 2nd Int. Conf. Recent Advances in Geotechnical Earthquake Engineering and Soil Dynamics, St Louis*, vol. 2, pp. 1079–1086.

Taylor, G. A. 1958 The 1951 eruption of Mount Lamington, Papua. *Aust. Bur. Min. Resources Geol. Geophys. Bull.* **38**, 1–117.

Terzaghi, K. 1950 Mechanisms of landslides. *Engineering geology (Berkey) volume.* Geological Society of America.

Tinti, S., Bortolucci, E. & Armigliato, A. 1999. Numerical simulation of the landslide-induced tsunami of 1988 on Vulcano Island, Italy. *Bull. Volcanol.* **61**, 121–137.

Ugai, K. & Leshchinsky, D. 1995 Three-dimensional limit equilibrium and finite element analyses: a comparison of results. *Soils Found.* **35**, 1–7.

Ui, T. & Fujiwara, H. 1993 Debris avalanche database. In *Scale and characteristics of volcanic disasters, prediction of natural disasters and prevention measures for society* (ed. S. Aramaki), pp. 177–188. Ministry of Education and Scientific Research Funding (Mombusho), priority area research report no. A-4–5 (in Japanese).

Van Bemmelen, R. W. 1949 *The geology of Indonesia.* The Hague: Nijhoff.

Van Bemmelen, R. W. 1950 Gravitational tectogenesis in Indonesia. *Geol. Mijnbou* **12**, 351–361.

Van Wyk de Vries, B. & Borgia, A. 1996 In *Volcanic stability of the earth and other planets* (ed. W. J. McGuire, A. P. Jones & J. Neuberg), vol. 110. London: Geological Society.

Van Wyk de Vries, B. & Francis, P. W. 1997 Catastrophic collapse at stratovolcanoes induced by gradual volcano spreading. *Nature* **387**, 387–390.

Van Wyk de Vries, B., Self, S., Francis, P. & Keszthelyi, L. 1999 Development of the Socompa debris avalanche (N. Chile) from a spreading volcanic edifice. *Eos* **80**, F1142.

Vermeer, P. A. (ed.) 1991 *Plaxis: finite element code for soil and rock plasticity.* Rotterdam: Balkema.

Vermeer, P. A. & De Borst, R. 1984 Non-associated plasticity for soils, concrete and rock. *Heron* **29**, 5–62.

Voight, B. (ed.) 1979 *Rockslides and avalanches, 2: engineering sites.* Amsterdam: Elsevier.

Voight, B. 1980 Slope stability hazards, Mount St Helens volcano, Washington. Technical report of the US Geological Survey. File report: Cascades Volcano Observatory, Washington. (See the report included at the end of this paper.)

Voight, B. 1981 Time scale for the first moments of the May 18 eruption. *Prof. Paper US Geol. Surv.* **1250**, 69–86.

Voight, B. 1988 A method for prediction of volcanic eruptions. *Nature* **332**, 125–130.

Voight, B. 1989 A relation to describe rate-dependent material failure. *Science* **243**, 200–203.

Voight, B. 1992 Causes of landslides: conventional factors and special considerations for geothermal sites and volcanic regions. *Geothermal Resource Council Trans.* **16**, 529–533.

Voight, B. 1996 Strength of wall rock of English's Crater, Soufrière Hills volcano, Montserrat. In *The Soufrière Hills eruption, Montserrat* (Abstracts), p. 29. Geological Society, 27 November 1996.

Voight, B. & Dahl, H. D. 1970 Numerical continuum approaches to analysis of nonlinear rock deformation. *Can. J. Earth Sci.* **7**, 814–830.

Voight, B. & Elsworth, D. 1997 Failure of volcano slopes. *Géotechnique* **47**, 1–31.

Voight, B. & Elsworth, D. 2000 Stability and collapse of hazardous gas-pressurized lava domes. *Geophys. Res. Lett.* **48**, 1–4.

Voight, B. & Kennedy, B. 1979 Slope failure of 1967–1969, Chuquicamata mine, Chile. In *Rockslides and avalanches, 2: engineering sites* (ed. B. Voight), pp. 595–632. Amsterdam: Elsevier.

Voight, B. & Sousa, J. 1994 Lessons from Ontake-san: a comparative analysis of debris avalanche dynamics. *Eng. Geol.* **38**, 261–297.

Voight, B., Glicken, H., Janda, R. J. & Douglass, P. M. 1981 Catastrophic rockslide avalanche of May 18. *Prof. Paper US Geol. Surv.* **1250**, 347–378.

Voight, B., Janda, R. J., Glicken, H. & Douglass, P. M. 1983 Nature and mechanics of the Mount St Helens rockslide-avalanche of 18 May 1980. *Géotechnique* **33**, 243–273.

Voight, B., Janda, R. J., Glicken, H. & Douglass, P. M. 1985 Nature and mechanics of the Mount St Helens rockslide-avalanche of 18 May 1980. Reply to discussion. *Géotechnique* **35**, 357–368.

Voight, B., Calvache, M. L & Ospina Herrera, O. 1987 High-altitude monitoring of rock mass stability near the summit of Volcano Nevado del Ruiz, Colombia. *Proc. 6th Int. Cong. International Society of Rock Mechanics, Montreal*, pp. 275–279.

Voight, B., Orkan, N. & Young, K. 1989 Deformation and failure-time prediction in rock mechanics. In *Proc. 34th US Symp. Rock Mechanics*. Rotterdam: Balkema.

Voight, B., Hoblitt, R. P., Clarke, A. B., Lockhart, A. B., Miller, A. D., Lynch, L. & McMahon, J. 1998 Remarkable cyclic ground deformation monitored in real time on Montserrat and its use in eruption forecasting. *Geophys. Res. Lett.* **25**, 3405–3408.

Voight, B. (and 24 others) 1999 Magma flow instability and cyclic activity at Soufrière Hills volcano, Montserrat, British West Indies. *Science* **283**, 1138–1142.

Wadge, G., Francis, P. W. & Ramirez, C. F. 1995 The Socompa collapse and avalanche event. *J. Volcanol. Geotherm. Res.* **66**, 309–336.

Wadge, G., Woods, A., Jackson, P., Bower, S., Williams, C. & Hulsemann, F. 1998 A hazard evaluation system for Montserrat. In *Forecasts and warnings*, ch. 3. UK Coordination Committee for IDNDR. London: Telford.

Wang, Y.-J. & Voight, B. 1969 A discrete element stress analysis model for discontinuous materials. In *Proc. Int. Symp. Large Permanent Underground Openings, Oslo*, artikkel 6. International Society of Rock Mechanics.

West, S. 1980 Earth sciences. *Science News* (20 December), p. 399.

Wiberg, N. E., Koponen, M. & Runesson, K. 1990 Finite element analysis of progressive failure in long slopes. *Int. J. Num. Analyt. Methods Geomech.* **14**, 599–612.

Williams, H. & McBirney, A. R. 1979 *Volcanology*. San Francisco, CA: Freeman, Cooper.

Yamamoto, T., Nakamura, Y. & Glicken, H. 1999 Pyroclastic density current from the 1888 phreatic eruption of Bandai volcano, NE Japan. *J. Volcanol. Geotherm. Res.* **90**, 191–207.

Young, S. R., Sparks, R. S. J., Aspinall, W. P., Lynch, L. L., Miller, A. D., Roberston, R. E. A. & Shepherd, J. B. 1998 Overview of the eruption of Soufrière Hills volcano, Montserrat, July 18, 1995, to December 1997. *Geophys. Res. Lett.* **25**, 3389–3393.

Zienkiewicz, O. C., Humpheson, C. & Lewis, R. W. 1975 Associated and non-associated viscoplasticity and plasticity in soil mechanics. *Géotechnique* **25**, 671–689.

B. Voight

SLOPE STABILITY HAZARDS,
MOUNT ST HELENS VOLCANO, WASHINGTON

Barry Voight

Submitted to:

US Geological Survey Investigation for
Mount St Helens Volcano   May 1, 1980

Federal Office Building

500 W. 12th Street

Vancouver, WA 98660

Attn: D. R. Crandell

Slope Deformation Mechanisms and Hazards

The principal hazard at Mt. St Helen's during the period of my observations (11–19 April, 1980) involved the potential instability of the north slope. The mountain crest in the north slope, including the area of the Boot, is crossed by a system of closely spaced uphill facing scarps of approximate east–west trend.

A ridge-top depression (trench) separates this fracture system from an approximately parallel system of fractures that cross the present summit and extend for perhaps a kilometer. The principal fractures of both systems dip to the north, perhaps at 40–50°. The rear (south)-scarp fracture system can be followed downslope to the northwest for a vertical distance of 500 m or so; to the northeast it is more difficult to follow, but there are suggestions that it crosses the mountain slope under Forsyth Glacier, west of the Dog's Head. The glacier is much crevassed and movements along crevasse systems are reflected in a series of systematically-oriented scarps, some of which face uphill. Part of the glacier deformation reflects deformation of the entire mountain face; part may be independent of the movements of underlying rock.

Crater development has proceded [sic] within the ridge-top depression, and some hydrothermal activity has been observed at several localities along the traces of the graben boundary faults.

The association of uphill facing scarps and ridge top depressions, where found elsewhere, have ordinarily been interpreted as manifestations of mass rock creep—gravitational rock deformation without the necessity for discrete sliding surfaces (i.e. 'Sackung'; Zischinsky, 1966). These features occur in a wide variety of settings, in heterogeneous or relatively homogeneous ground, and with or without the influence of anisotropy. Their specific mechanisms are not well understood, and indeed various mechanisms are likely involved in different settings. Most localities occur in seismically active regions, and earthquake vibrations probably play a significant role in many cases, including Mt. St Helens. At Mt. St Helens are additional complications, of course, associated with inflation and deflation of magma chambers and hydrothermally pressured domains. These make the mechanism problem at St Helens especially involved, and carefully obtained data from slope monitoring installations will probably be necessary in order to resolve the issues. As an example, the ridge top depression at St Helens might be interpreted as a localized extensional strain feature resulting from cyclic, hydraulically-generated inflation of the volcanic edifice (related
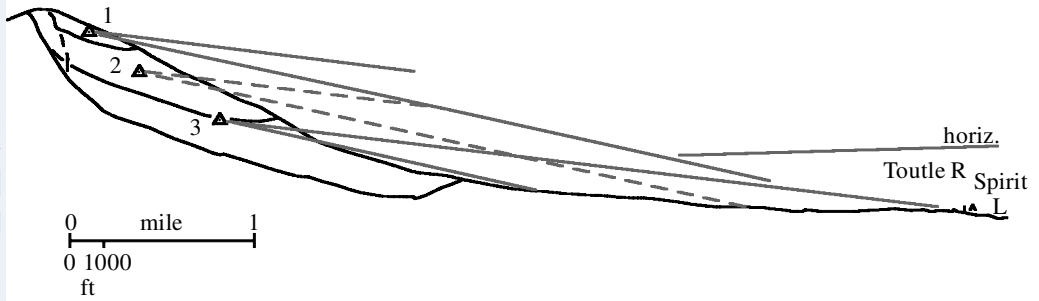
Figure 15. Potential slide profiles for velocity calculations.

to stream [sic; steam] eruptions). The graben faults do not recover their displacements during the following deflation part of the cycle because of friction; deformation of the edifice is thus locally 'plastic', i.e. incompletely recoverable. A consequence is that intergranular horizontal compressional stresses arise in the edifice, normal to the strike of the ridge top depression during periods of deflation—inasmuch as the stretched 'surface length' of the edifice cannot now fully decompress to its original form. These horizontal stresses can in turn cause basal failure along weak strata at depth, perhaps thereby leading to detachment of a major rockslide.

In some cases elsewhere, interpretations of ridge-top trenches and related phenomena as manifestations of rock creep 'sagging' have been debated, e.g. because of an apparent lack of bulging in lower parts of a given slope. However, the amount of valleyward bulging necessary to accommodate the strains indicated by ridge top grabens is in most cases small. Careful slope displacement monitoring, <u>not</u> visual observations, are ordinarily required to assess the issue. Little 'hard' data of this kind in fact exist.

In the United States such 'gravitational' features have not been traditionally well studied, but recent reports by R. W. Tabor (1971) in the nearby Olympic Mountains, and by D. H. Radbruck-Hall and co-authors (1978, 1976), have improved the state of our knowledge.

In some locations ridge crest grabens mark the head of large rockslide blocks, and the uphill facing scarp faults intersect the principal slideblock movement surface at depth. This is still a possibility for St Helens, and an important one. I observed no specific connection between the graben faults and any 'basal' rockslide slip surface or zone, <u>but</u> a veneer of snow, ice, and ash hides much of the slope, and it is possible that such a connection would exist and yet be unobserved at the present time. Furthermore, even if no basal slip-surface exists at present, one could develop in the future, perhaps in conjunction with hydraulic pressures generated in quasi-continuous porous fragmental layers which make up much of the edifice beneath the surface. Local dome plugs and other igneous intrusions within the fragmental edifice are likely to be highly fractured and probably offer little in the way of cohesive 'buttress reinforcement' that would prevent development of a rockslide slip surface.

A most dangerous future condition would involve the saturation of fragmental layers by hot water, and rapid transmission of hydraulic explosive pressures generated at the volcano throat throughout a critically located saturated layer.

A rockslide triggered by such an event could be as much as a kilometer thick and involve a cubic kilometer or more of rock and fragmental material; emplacement
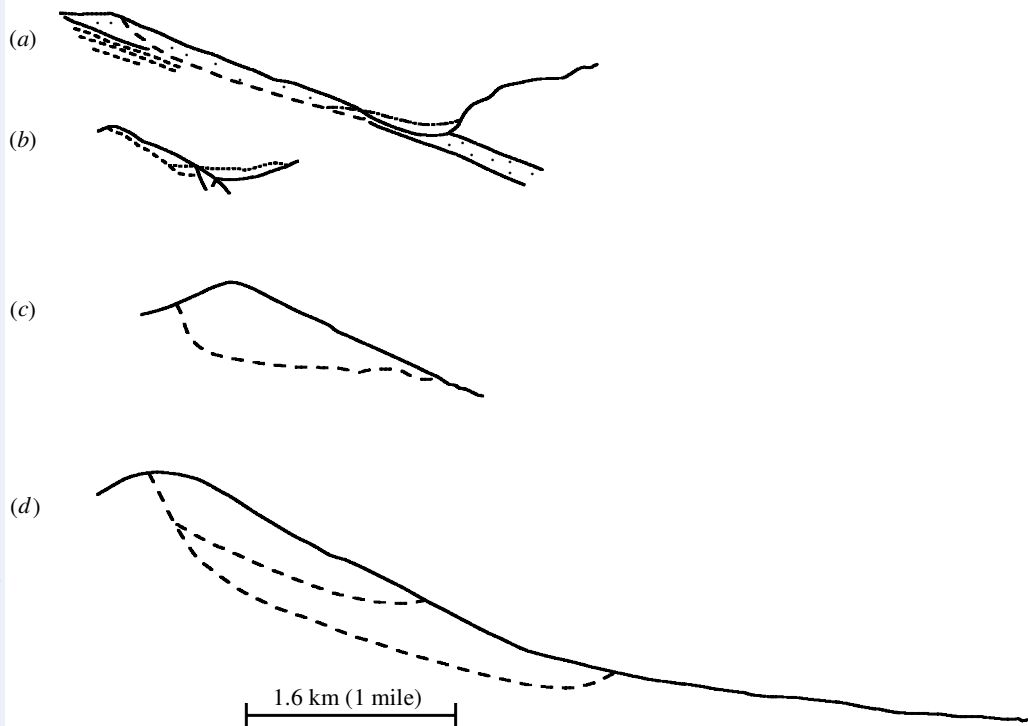
Figure 16. Comparison of profiles for (*a*) Gros Ventre slide, (*b*) Madison Canyon slide, (*c*) Bandai-san volcano, (*d*) Mt. St Helens. Scale is identical for all figures.

velocities valleyward on the order of 100 km/hr are possible, with the mass breaking up and descending as a debris flow to the Toutle River Valley [figure 16].

Relief of overburden pressure caused by slip of the rockslide mass would likely promote further explosive activity (flashing) in hydrothermal systems occupying the core of the volcanoe [sic] and the surrounding porous edifice, and perhaps also in shallow magma chambers. A catastrophic event of the kind observed at Bandai-San—in which an explosively-motivated fragmental flow devastated an area of more than 70 km^2 (27 mi^2)—must be regarded as a legitimate possibility, particularly in view of the enhanced hydraulic pressure conditions implied by frequent summit steam explosions and the relatively high level of released seismic energy [see figures 16–18].

On the more prosaic side, a bulging slope associated with rock creep (increased tilt) may lead to an increase of rockfall hazards from exposed rock areas such as Goat rocks, increased snow avalanche hazard, and increased risk of glacier falls.

Glacier Avalanche Hazards

This is a distinct possibility at Mt. St Helens. The following mechanisms could promote it:

(1) Geothermal systems with subglacial outlets promote abnormally high basal melting, leading to 'lubrication' of the basal surface, separation of ice from rock, and high basal pore water pressures.
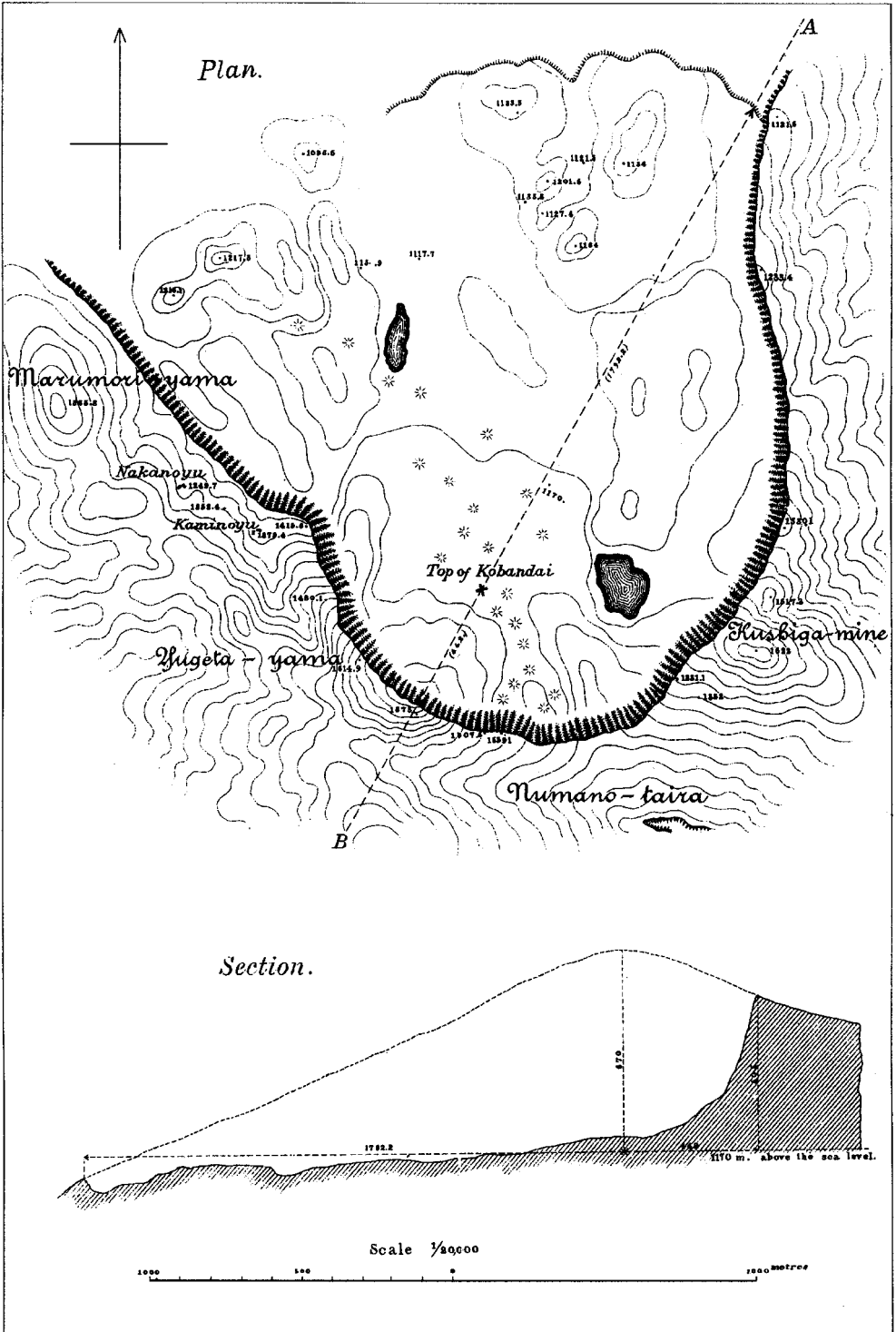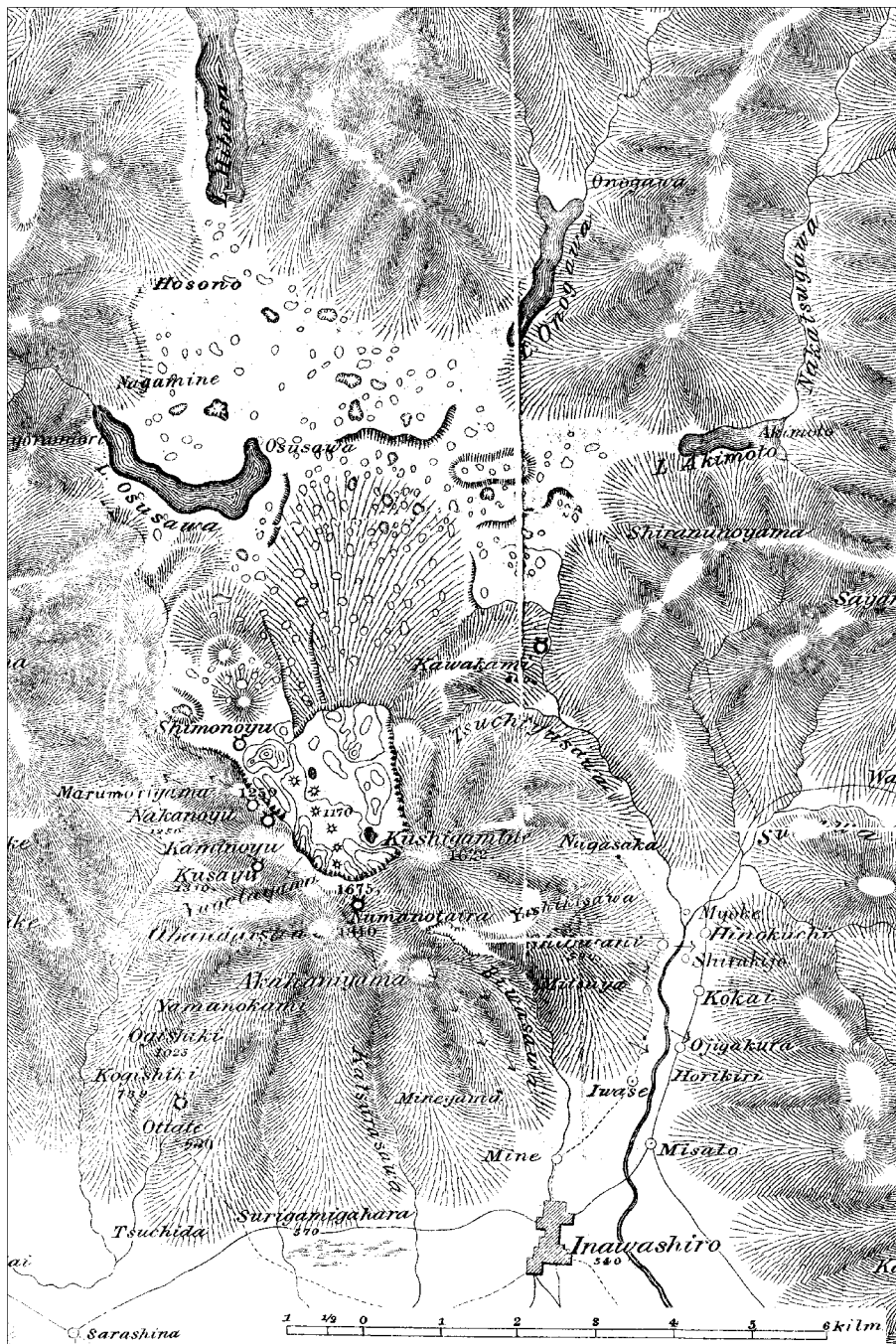
Figure 17. Bandai-san map and profile.

Figure 18. Bandai-san regional map of devastated area.

(2) Enhancement of regelation and creep response by added heat flow.

(3) Seismic damage of 'cohesive' areas involving glacier ice and bedrock knobs.

(4) Transient seismic shear stresses.

(5) Deformation of glaciers as part of the north slope rock deformation pattern.

(6) Tilt associated with bulging basal slope.

(7) Locally increased glacial surface slope, associated with enhanced glacier creep rate (due, in turn, to mechanisms (1)–(5)).

The glaciers most likely to be so affected include Toutle and Nelson glaciers, and those on the north slope which lie between them. In particular, the fracture patterns and surface configuration of Forsyth glacier suggests that it has been disturbed. It is probably deforming (creeping) independently of the bedrock trough in which it lies, and constitutes a distinct hazard to the Timberline campground area. Accordingly, only essential operations should be carried out in this area.

As an example of this kind of hazard a glacier avalanche represents a few pages are appended from the report of Slingerland and Voight (1979), on the Fallen Glacier event of 1905 [the appendix, consisting of pp. 376–380 from the original source, is omitted here]. Velocity calculated for the avalanche front is 60 m/s. The avalanche spread out along a front twice its initial width, entered a body of water, and produced wave run-ups over 100 ft high.

Hazards at Graben Boundaries

The possibility of breakdown of volcanic walls at the graben boundaries should be recognized. Hydrothermal activity is present along portions of the exposed west flank graben fault system. Internal collapse and lateral hydraulic erosion (piping) along these graben faults could lead to the rapid release of a significant flow of water from the crater plumbing system. The result would be mobilization of a (hot) lahar descending directly down the valley of the South Fork Toutle River. A similar event could occur on the northeast flank; here it would probably be preceded by a glacier avalanche.

Wave Runup Hazards

A hazard exists for Spirit Lake, which is within reach of a large, low effective friction, rockslide-avalanche from Mt. St Helens, and for the reservoirs on the south flank, notably Swift Reservoir, within reach of mudflows from St Helens. Although the present hazard assessment emphasizes north slope deformation, movement of mudflows to the south would also be possible. At Bandai-San also, the main explosive event occurred to the north, but large, damaging debris flows also extended south from the mountain summit.

The fragmental flows could enter these water bodies at high velocities, e.g. $\sim$ 50 km/hr, producing wave amplitudes on the order of the water depth in the slide impact area. The water wave train would then move at a velocity (celerity) equal to $\{g(d+\eta)\}^{1/2}$, where g is acceleration of gravity, d is water depth, η is wave amplitude. Runup could be significantly in excess of deep water wave amplitude.

Velocity and Runout

The simplest model for dynamic slide behavior concerns a block on an inclined plane. Friction between block and plane prevents sliding below a critical angle of inclination. Above this angle the mass accelerates according to Newton's second law. Deceleration occurs on lesser slopes. If the dynamic analysis is carried out from slide initiation to cessation of motion, $h = d \tan \phi$, where h is the vertical drop, d is horizontal distance moved, and ϕ is the apparent friction angle. Therefore the inclination of a line drawn between the starting and stopping points of the mass center of the block is ϕ, the friction angle. If the ground profile should project above this line at any point, the slide must stop at the point of intersection between the line and ground profile. Thus velocities, runout, and travel times are completely determined within the confines of the model. Motion of the mass center of a deformable body translates according to Newton's second law, so that in this respect the block model is still appropriate as a conceptual guide.

However, the actual mechanisms of slide motions are poorly understood, so that 'measured' friction values are not in general directly applicable. In the absence of reliable site-specific measurement procedures it is appropriate to use apparent friction values back-calculated from published slide profiles. An 'average' value of $\tan \phi$ determined in this way is about 0.25, with a 'lower-bound' value approximately 0.15. Corresponding friction angles are 14° and 9°, respectively. Three north slope slide models, relatively of small, medium, and large size, are considered [figure 15]. If $\phi = 14°$, model 3 (the largest) will move over a mile, but not much farther. The massive slide front will not reach Spirit Lake or Toutle River (discounting mobilized portions of the slide front which might continue as debris flow lobes). Model 2 could run for perhaps three miles, with frontal lobes barely reaching the Toutle River, and model 3 could run over four miles.

Velocities (V) may be calculated from

$$V = V_0 + gt(\sin i - \tan \phi \cos i)$$

or,

$$V = V_0 + \{2gs(\sin i - \tan \phi \cos i)\}^{1/2}$$

where V_0 is initial velocity, t is elapsed time, g is gravitational acceleration, i is slope angle, ϕ is friction angle, s is distance traveled. For example, for slide mass 2, letting $i = 19°$, $s = 2560$ m, $\tan \phi = 0.25$, $V_{\max} \approx 67$ m/s, at the break in slope. For the same point and $\tan \phi = 0.15$, $V_{\max} \approx 96$ m/s, which illustrates the sensitivity of the friction factor.

On these grounds it may be noted that the largest potential slide masses are not necessarily the most hazardous. For constant friction, an inverse relation exists between slide size and runout (and maximum velocity), principally due to the decreased elevation of mass centers in the larger potential slide masses.

On the other hand, small slides—despite their high potential velocity—will not have the height nor mass to overrun the forest cover below timberline; the principal hazard from such slides or avalanche events will be felt above timberline and in unforested chutes and valleys extending to lower elevations. Furthermore, for catastrophic slides there may be a correlation between increased slide volume versus

decreased apparent friction angle. With a decreased friction angle (say 9°) the earlier slide masses could reach the Toutle River valley, with energy to spare. (The best indicators of the limits of hazardous areas are not, incidentally, to be gained from calculations such as these, but rather from what has been observed from study of older deposits).

The above considerations have involved comparisons to simple rockslide and avalanche events elsewhere. The dynamic problem is compounded by considering the possible effects of pressurized steam, suddenly released and distributed throughout a cubic kilometer or so of fragmental material, potentially leading to a rapid mass torrent on an almost unprecedented scale. The obvious analog is the 1888 Bandai-San deluge of rock and earth, which buried a landscape over 70 km^2 in areal extent (Sekiya & Kikuchi, 1888) [figures 16 and 17].

Monitoring and Warning System

The following are some notes on instrumentation and monitoring, written in large part during my tenure in Vancouver, and aboard the flight east. I include them here in order to establish a benchmark from my perspective at this time, so that future workers may more easily advance further in these matters.

Slope hazards at St Helens are legitimate causes for concern. They need to be viewed from appropriate time perspectives; these perspectives must include immediate needs, and long-range needs (the period of concern may last 20 years).

A slope hazard monitoring plan should be developed; this should include consideration of (1) instruments and monitoring devices; (2) their installation; (3) monitoring (data gathering) program; (4) data processing program; (5) implementation, in terms of contingency plan.

It may be desirable to consider the establishment of a 'Hazard Monitoring Review Board' to consider these matters more thoroughly, and to provide necessary continuity to the program over a period of years or decades.

As regards a monitoring program for hazard evaluation, it is well to note at the outset that 'hazard warning monitoring' and 'scientific' monitoring (i.e. volcanic behavior) programs may substantially differ. Some overlap and coordination of the two programs is undoubtedly necessary at St Helens, but the goals and means of obtaining them are distinctly different. Instruments and systems suitable to one effort will not necessarily be satisfactory to the other. As a result, care needs to be given to an administrative structure that will govern funds and recognize the special needs of the hazard monitoring effort in an effective manner.

As regards methods, it is clear that high frequency or continuous displacement monitoring is the most effective means for slope failure prediction. If significant increases in slide velocity are detected, the indication is that the shear strength of some portion of the rock mass has been reduced; slope collapse could then be the ultimate consequence.

At Chuquicamata (an open pit mine in Chile, commonly cited for an example of successful rock slide prediction), an estimate of 'maximum displacement' was used as an instability criterion. Actual slope failure occurred on the earliest of a range of predicted dates, thus inferred from displacement measurement. The main lesson is that by knowing what to look for, and making complete use of available data, a set of sound decisions were made, thereby avoiding serious consequences which could

have resulted from an unanticipated slope failure. One could hope for no more than this at St Helens (cf. Voight and Kennedy, 1979).

The use of displacement monitoring for hazard prediction emphasizes once again the importance of establishing on an absolutely <u>sound basis</u> the control for a program of conventional surveying. As I have previously mentioned, this should be accomplished by professionals, not by scientists (however competent) whose duties are compromised by numerous other tasks of greater ultimate interest to them. The ground control will serve as a basis for all future deformation measurements, over a period of decades; it is absolutely imperative that they be initially dealt with by a state-of-the-art approach. Both air and terrestrial photogrammetry are advisable for displacement data acquisition. Analytical Photogrammetric measurement generally requires a control survey carried out prior to photography to establish coordinates of a number of points in the field of view. Reference may be made to my memos of 14 and 19 April 1980 concerning procedures, knowledgeable specialists, and local contacts.

As regards installed devices, I anticipate that P. Douglass will place the program which I began on a much firmer basis, with due consideration of adequate markers, crack gauges, and the like.

Some random advice: (1) the number of instruments installed should allow for a percentage of future instrument losses and failures, (2) a large number of widely distributed, cheap, crude, but reliable devices is usually better than a few very sensitive, expensive instruments; (3) a common error is to underestimate the realistic duration of the project. This factor reflects upon the durability and relative 'permanence' of monitoring devices and on budget requirements necessary to ensure an appropriate frequency of measurement. Devices placed in order to satisfy immediate needs may need to be replaced as time permits by more durable designs; (4) the 'graben' deformation should be closely watched and measured, inasmuch as this feature is intrinsically a displacement and strain gauge of sorts.

The depth to the potential basal slide plane probably precludes the use of ordinary borehole instrumentation systems, such as extensometers, tiltmeters, and shear strips. Water pressure monitoring in deep borehole[s] on the flanks of the mountain would be of interest; this would be costly and only an indirect indication of stability conditions in the slope, but may be nevertheless worthwhile as a long range task.

As data becomes available automated warning systems should be considered. They are of value if they are reliable, transmit data rapidly, and are designed with respect to a reasonable slope failure criterion and risk analysis. If the warning is clear cut, the action must be prompt. Hazard warning systems could become part of the St. Helens contingency plan, with various specified actions dependent upon the achievement of pre-set hazard warning levels. In this regard the establishment of a 'Hazard Monitoring Review Board' may be recommended as a means to avoid the delays and costs of formal reporting of results that are intended as the basis for action.

Potential results of a monitoring system are as follows: the displacement magnitude, direction, rate, and rate change, for points of specific interest, distributed over the slope (within and outside of the potential failure zone). Mechanisms are inferred from the evidence on displacement. The extent of the (potentially) unstable mass is given by displacements and inferred mechanisms, leading to estimates of rock mass volumes, and predictions in potential slide dynamics (velocities, runouts) based on mass center location.

As regards the specific prediction of impending slope failure, fundamental problems are involved. The problems do not so much involve data acquisition, but rather the establishment of specific predictive criteria marking the onset of catastrophic sliding. At St Helens a preliminary problem involves the separation of observed displacement components, i.e. distortion of the volcanic edifice, vs. 'gravitational' deformation. To the extent that the involved mechanisms may be intertwined, this in itself could prove difficult. Assuming that this matter can be resolved, important questions remain: (1) how can movements which occur in slopes that collapse be distinguished from those in slopes that stabilize?; (2) If advance prediction of failure is needed, what extrapolation method for movements is most suitable?; (3) What criterion is a reliable predictor of slope failure?

Information on time rates of deformation are difficult to incorporate directly into rational descriptions of stability conditions. This is a weakness in geotechnical monitoring-design schemes for rock slopes, but there is no easy way to surmount the problem. The result is that intuition and experience are essential factors in drawing sound conclusions from geotechnical deformation measurements.

References

Pariseau, W. G., and Voight, B., 1979, Rockslides and avalanches: Basic principles, and perspectives in the realm of civil and mining operations, p. 1–92, in Voight, B., Ed., *Rockslides and Avalanches, 2. Engineering Sites.* Elsevier Scientific Publishing Co., Amsterdam, 850 pp.

Radbruch-Hall, D. H., 1979, Gravitational creep of rock masses on slopes, p. 607–657, in Voight, B., Ed., *Rockslides and Avalanches, 1. Natural Phenomena.* Elsevier Scientific Publishing Co., Amsterdam, 833 pp.

Radbruch-Hall, D. H., Varnes, D. J., and Savage, W. Z., 1976, Gravitational spreading of steep-sided ridges ('Sackung') in western United States. *Bull. Int. Assoc. Eng. Geol.*, 14: 23–25.

Sekiya, S. and Kikuchi, Y., 1889, The eruption of Bandai-san, *J. Coll. Sci. Tokyo Imp. Univ.*, 3: 91–172.

Slingerland, R. L. and Voight, B., 1979, Occurrences, properties, and prediction models of landslide-generated water waves, p. 317–397, in Voight, B., Ed., *Rockslides and Avalanches, 2. Engineering Sites.* Elsevier Scientific Publishing Co., Amsterdam, 850 pp.

Tabor, R. W., 1971, Origin of ridge top depressions by large-scale creep in the Olympic Mountains, Washington, *Geol. Soc. Am. Bull.*, 82: 1811–1822.

Voight, B. and Kennedy, B. A., 1979, Slope failure of 1967–1969, Chuquicamata Mine, Chile, p. 595–632, in Voight, B., ed., *Rockslides and Avalanches, 2. Engineering Sites.* Elsevier Scientific Publishing Co., Amsterdam, 850 p.

Zischinsky, U., 1966, On the deformation of high slopes. *1st Congr. Int. Soc. Rock Mech.*, Lisbon, 2: 179–185.

[Notes: The above manuscript is unaltered and several typographical errors of the original are unrepaired, although noted by comments within square brackets. The table of contents and appendix of the original have been omitted. Figure references are added in brackets. (See also figure 4 of preceding article.)]